VILNIUS UNIVERSITY

Life Sciences Center

Institute of Biosciences

Neurobiology Master‘s course, II year student

Viktoras MAŽEIKA

Master’s thesis

Investigation of the potential use of $CuInS_2/ZnS$ quantum dots for brain cancer diagnostics

Supervisor:

Dr. V. Karabanovas

Consultant:

PhD student D. Dapkutė

Vilnius, 2020

Investigation of the potential use of $CuInS_2/ZnS$ quantum dots for brain cancer diagnostics

Thesis prepared at

National Cancer Institute, Biomedical Physics Laboratory

Viktoras MAŽEIKA _____

Supervisor:

Dr.V. KARABANOVAS _____

Consultant:

PhD student D. DAPKUTĖ _____

Abbreviations

aQDs – aminated $CuInS_2$/ZnS quantum dots

AFM – atomic force microscopy

Ce6 – chlorin e6

CIS – $CuInS_2$

CNT – carbon nanotube

CNS – central nervous system

cQDs – carboxylated $CuInS_2$/ZnS quantum dots

CT – computed tomography

DMEM – Dulbecco's modified Eagle's medium

DLS – dynamic light scattering

FBS – fetal bovine serum

FL – fluorescence lifetime

FRET – Förster resonance energy transfer

GO – graphene oxide

MRI – magnetic resonance imaging

NP – nanoparticle

NS cancer – nervous system cancer

OCT – optical coherence tomography

QD – quantum dot

PBS – phosphate buffered saline

PDT – photodynamic therapy

PL – photoluminescence

PNS – peripheral nervous system

PTT – photothermal therapy

TABLE OF CONTENTS

INTRODUCTION

Cancer is one of the leading causes of death worldwide, so researchers are always on the pursuit for new diagnostic and therapeutic methods or ways to improve the effectiveness of those already in use. Quantum dots, a type of nanomaterial, could be used both to enhance sensitivity of optical methods, such as fluorescence spectroscopy, and enable several therapeutic methods, like photodynamic therapy (Lucky et al., 2015; Smith and Gambhir, 2017). Unique properties of quantum dots could be especially useful for targeted theranostics of nervous system tumors. Clinical visualization systems based on quantum dots could be used intraoperatively as a visual aid for surgeons and photodynamic therapy has potential for treating some types of brain tumors which cannot be effectively treated with conventional methods (Perkins and Liu, 2016; Vasefi et al., 2016). Even more importantly, quantum dots, alongside other nanomaterials, can be tailored to allow for crossing of the blood-brain barrier, thus providing a means to solve this long-standing problem of brain cancer therapeutics (Li et al., 2017). One drawback of commonly used quantum dots – their inherent nanotoxicity – can be circumvented by using heavy metal-free quantum dots, such as those made from $CuInS_2$ (Pons et al., 2010). The use of these quantum dots for nervous system cancer theranostics has not been extensively investigated, so such research is of the utmost importance if these nanoparticles are to be applied clinically.

The aim of this work – to investigate the potential use of heavy metal free $CuInS_2$/ZnS quantum dots for brain cancer diagnostics.

Tasks of this work:

1. To investigate the optical and physicochemical properties of $CuInS_2$/ZnS quantum dots functionalized with amine or carboxyl functional groups;

2. To compare the stability of $CuInS_2$/ZnS quantum dots in different media;

3. To investigate the accumulation of $CuInS_2$/ZnS quantum dots in cancer cells and their effect on cell viability.

1. LITERATURE REVIEW

1.1. Nervous system cancer, its diagnostics and treatment

1.1.1. Nervous system cancer and its classification

Cancer is a group of diseases caused by mutations in certain genes which induce cells to divide uncontrollably and, in the case of malignant tumors, invade nearby healthy tissue. Various types of cancer are one of the leading causes of death worldwide, second only to cardiovascular diseases, especially in developed countries (Naghavi et al., 2017). Due to this, cancer research is one of the most active and well-funded fields of medical research. Researchers are trying to expand their understanding of the causes of different cancer types, as well as to discover better diagnostic methods, which would allow to detect cancer at its early stages, and create more effective types of treatment, which could efficiently treat cancer while causing as little harm to the patient as possible.

Nervous system (NS) cancer, as the name suggests, is a type of cancer originating from nerve or glial cells. Such tumors may form in central (CNS) (brain or spinal cord) or peripheral nervous system (PNS). Symptoms vary depending on the location of the tumor and may include headaches, seizures, loss of consciousness and various neurological symptoms, such as sensory, motor, language and cognitive deficits or even behavioral changes in the case of CNS tumors (McFaline-Figueroa and Lee, 2018). PNS tumors mainly cause pain and sensorimotor deficits (Huang et al., 2005). These symptoms can be caused by either benign or malignant tumors, so even if there is no danger of further cancer development, treatment of such tumors may be necessary.

NS tumors can be classified by their location, cellular origin or molecular characteristics. Although currently it is recommended to classify NS tumors according to their molecular characteristics (Louis et al., 2016), a more intuitive classification based on their cellular origin will be presented. Considering only primary tumors (that is, tumors not grown from metastatic cancer cells from other body parts), main types of NS tumors are gliomas, meningiomas, pituitary tumors and nerve sheath tumors, although there are some more types than the ones listed. Gliomas are tumors originating from glia precursor cells. They are one of the most common types of primary brain tumors and are the most common malignant type, with glioblastoma being the most lethal. Gliomas are classified into oligodendrogliomas,

astrocytomas, ependymomas and oligoastrocytic gliomas according to the resemblance between their cells and glial cells. Some types of gliomas may invade tissue diffusively, thus complicating treatment (Weller et al., 2015). Meningiomas originate from meninge cells and, although technically not being brain tumors due to not originating from neurons or glial cells, are categorized as such because they cause similar symptoms. This is the most common type of brain tumors, even though often they go unnoticed because of being benign and presenting no symptoms (DeAngelis, 2001). Pituitary tumors originate in the pituitary gland. They are similar to meningiomas in the way of often being benign and asymptomatic. In some cases, pituitary tumors can alter production of pituitary hormones and cause various symptoms, ranging from infertility and osteoporosis to diabetes (Molitch, 2017). Nerve sheath tumors affect cells producing the myelin sheath or cells of connective tissue. Schwannoma and neurofibroma are members of this type. They are mostly benign but may cause pain due to being close to peripheral nerves (Huang et al., 2005).

1.1.2. Problems associated with nervous system cancer diagnostics and treatment

Majority of NS cancer diagnostic methods are the same as those used for other types of cancer. Magnetic resonance imaging (MRI) with gadolinium as a contrast agent is the most commonly used due to its tissue specificity, while computer tomography (CT) can be substituted if MRI cannot be used for some reason. CT can also allow to detect primary tumors in other body parts if the tumor in the brain is metastatic. If diagnosis using these methods is not clear, biopsy or surgical resection can be performed, and it is the primary method used to determine the exact type of tumor (McFaline-Figueroa and Lee, 2018). Magnetic resonance spectroscopy, positron emission tomography, analysis of cerebrospinal fluid and some other methods, while not common, can also be used (American Society of Clinical Oncology, 2019). Treatment of NS tumors involves surgery (when it is possible to remove the tumor without causing damage to brain or other parts of nervous system) followed by radiotherapy and chemotherapy. Chemotherapy and radiotherapy (or its varieties, brachytherapy and stereotactic radiosurgery) can be used by themselves as well when surgery is not possible or the tumor is diffuse (Perkins and Liu, 2016). Surgery is effective with benign tumors, while malignant ones show a high probability of reoccurrence.

Even though mentioned diagnostic and treatment methods of cancer have seen withstanding successful clinical use, they do have some drawbacks. MRI and CT equipment is expensive, and the running costs are also quite high. In addition, while they are routinely

used extraoperatively, intraoperative use, allowing surgeons to use the image of tumor for guidance during surgery, remains difficult. MRI and ultrasound imaging, two methods used for this purpose, require expensive equipment and are time consuming or have inadequate sensitivity for imaging of small tumors, respectively. In addition, both methods require the surgeon to have plenty of experience to be able to accurately interpret the images (Vasefi et al., 2016). Chemotherapy and radiotherapy are associated with side-effects, potentially quite severe, and surgery is not always feasible. Even then, remission rates of certain brain cancers are high, with low 5 year survival rates (Bray et al., 2018) (Fig. 1.1.). These disadvantages call for new diagnostic methods, which would address these issues.

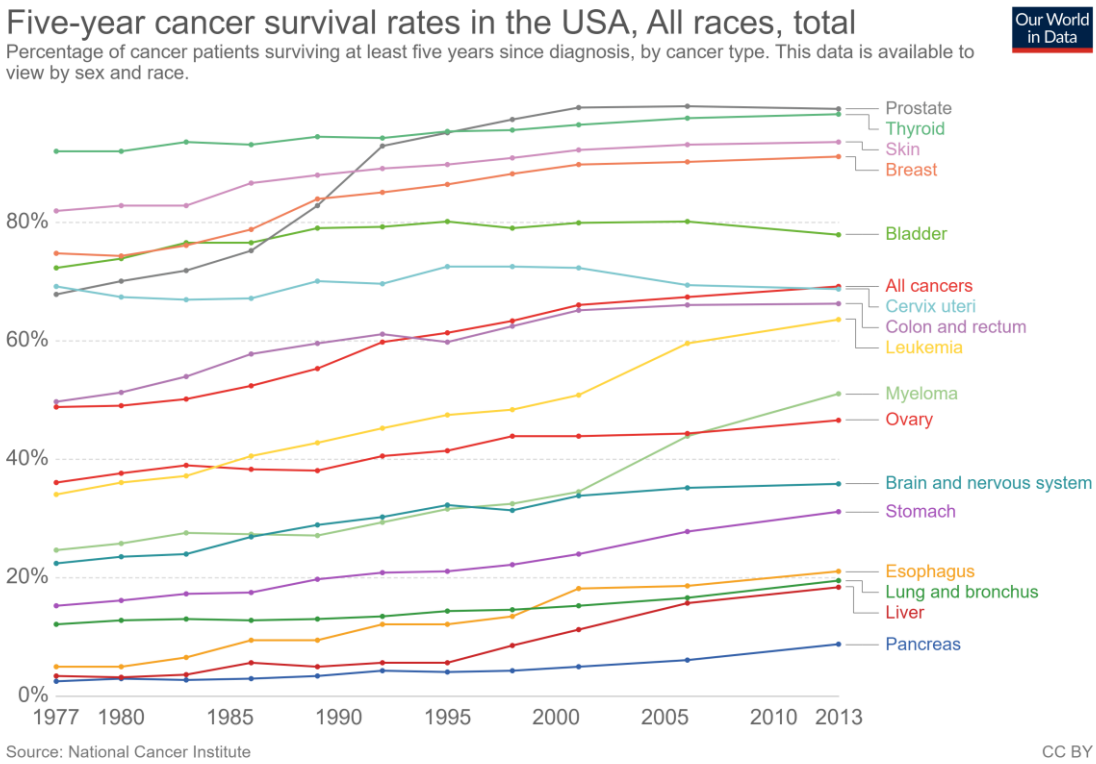

Figure 1.1. 5-year survival rates for different types of cancer, including brain and NS cancer, in the USA from 1977 to 2013 (Roser and Ritchie, 2018).

1.2. Optical methods for nervous system cancer diagnostics and therapy

1.2.1. Application of optical methods for nervous system cancer diagnostics

Optical methods, such as fluorescence spectroscopy, Raman spectroscopy or two-photon spectroscopy have seen extensive use in both *in vitro* and *in vivo* medical research. Such imaging methods are also investigated for use in diagnostics of NS cancer – for

example, Raman spectroscopy was capable to image glioma tumors during surgery and even differentiate tumor grades (Jermyn et al., 2015), while multiphoton tomography and fluorescence lifetime spectroscopy was used to the same effect during glioblastoma surgery (Kantelhardt et al., 2016). Optical methods have many advantages over MRI, CT and other currently used imaging methods: equipment required is generally not overly expensive, they are simple to use, allow real time imaging and acquired images are quite straightforward to interpret (Vasefi et al., 2016). In addition, optical methods are highly versatile and can be tailored for various imaging applications, including fluorescent probes having specificity for cancer cells (Garland et al., 2016). Improved specificity is an important advantage over radionuclide labeling, another method capable of real time imaging (McHugh et al., 2018). Optical methods could also be used for more advanced imaging applications, such as tracking the distribution of anti-cancer drugs (Kong et al., 2018).

1.2.1.1. Fluorescence spectroscopy

Both steady-state and time-resolved fluorescence spectroscopy can be used for tumor detection – the former investigates differences in spectral profiles and intensities between cancerous and healthy tissues, while the latter is used to compare changes in fluorescence decay times. Autofluorescence of tumor tissues and fluorescent probes binding to cancer cells can be utilized to detect tumors with these methods. Changes in tumor metabolism lead to differences in fluorescence spectra of amino acids (tryptophan and tyrosine), proteins (elastin, collagen) and some other compounds (NADH, FAD) compared to their spectra in healthy tissue (Vasefi et al., 2016). While in theory autofluorescence seems as a convenient way to detect tumors, numerous problems, such as low fluorescence intensity, complicated interpretation of images and possible interference from patient's diet and other factors limit its use. Fluorescent probes are employed to account for these drawbacks. Both targeted probes, which contain antibodies or various smaller peptides binding to tumor cells, and non-targeted ones (for example, indocyanine), instead relying on specifics of tumor vasculature , are used (Solomon et al., 2011).

Main advantages of steady-state fluorescence are low cost of equipment and higher signal quality compared with time-resolved spectroscopy. On the other hand, fluorescence intensity measurements can be distorted by numerous unrelated chemical compounds, as well as other factors, such as patient's motion during measurement or photobleaching. As time-

resolved techniques are not based on intensity measurements, they pose a solution to these problems (Solomon et al., 2011).

In brain cancer diagnostics, most of the recent research involving fluorescence spectroscopy involves its application as an aid during surgery or biopsy. Although biopsy is an important tool used to diagnose cancer, it is rather risky, and fluorescence spectroscopy is investigated as a visual aid during this procedure. This application was investigated by Haj-Hosseini et al., as a combination of fluorescence spectroscopy and laser Doppler flowmetry. A probe integrating both methods was employed. Researchers found the method effective, especially in combination with simultaneous autofluorescence measurements (Haj-Hosseini et al., 2018). Fluorescence probes are investigated for use in surgeries, too, as they allow for easier access to tumors. A comparison of such a probe with conventional fluorescence microscopy during surgery in the marginal zone of glioma found the probe to be more sensitive, as it could detect tumor remnants in two thirds of investigated spots where microscopy did not detect them (Richter et al., 2017). Of course, surgery is not the only investigated area of the application of fluorescence spectroscopy – one example is the research of Zhou et al., who used this method to determine the grade of tumors. Results showed that the method might be a viable alternative to currently used histopathological techniques. The experiments were conducted *ex vivo*, though, so it is not clear whether the method would be appropriate for *in vivo* use as well (Zhou et al., 2019).

1.2.1.2. Two-photon fluorescence spectroscopy

If suitable conditions are met (sufficient spatial localization of laser light, high laser power), a phenomenon called two-photon absorption can take place, which is basically absorption of two lower energy photons that excites a molecule into a higher energy state. This principle can be applied in a technique called two-photon fluorescence spectroscopy. Its main advantage over conventional fluorescence spectroscopy is the use of near-infrared light, which is less absorbed by tissue compared to visible light. In principle, this allows imaging of deeper tissue. Parallel with fluorescence spectroscopy, both endogenous and exogenous fluorophores can be used in two-photon fluorescence spectroscopy investigations, and most of the endogenous compounds used in one method are applicable in the other as well. This method's main drawback is a higher cost of equipment compared with the cost of steady-state fluorescence setup (Perry et al., 2012).

In, principle, application of two-photon fluorescence spectroscopy is similar to conventional fluorescence spectroscopy. In its simplest form, it can be used alone for detection of tumors, as shown in the work of Li and coworkers, where they used two-photon fluorescence lifetime spectroscopy to detect various tumors, brain tumors in mice among them. They found several differences in spectra of healthy and malignant tissues, which could be used for their discrimination (Li et al., 2019). More complex applications include combinations of several detection techniques. One investigation used two-photon spectroscopy together with second harmonic generation imaging and conventional single photon fluorescence spectroscopy, with the idea of the experiment being to use all these methods to facilitate discrimination of healthy and malignant tissue. Results seem positive, and researchers hope to apply this method to investigations of different brain tumor types, like glioma and meningioma (Fig. 1.2.) (Poulon et al., 2017).

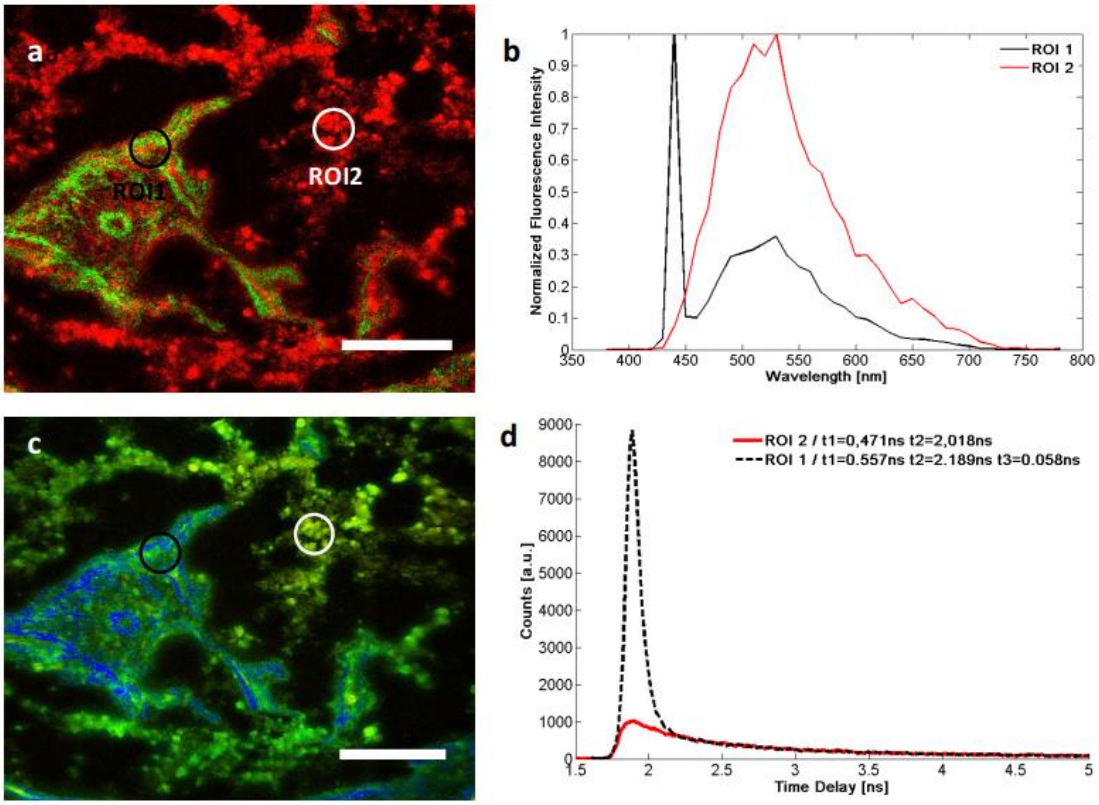

Figure 1.2. Comparison between two locations of metastatic tissue: a) Combined two-photon fluorescence and second harmonic generation image of metastatic tissue; b) fluorescence intensity spectra of ROI 1 (stroma) and ROI 2 (adenocarcinomatous glandular tissue); c) two-photon excitation fluorescence lifetime image of metastatic tissue; d) fluorescence lifetime decay curves of ROI 1 and ROI 2. Scale bar – 20 μm (Poulon et al., 2017).

1.2.1.3. Raman spectroscopy

Raman spectroscopy is a method of vibrational spectroscopy which detects energy changes of inelastically scattered photons. Most scattered photons are of the same energy (wavelength) as the impending ones, but in some instances their energy may change (either increase or decrease) by an amount corresponding to a vibrational energy level of a molecule. As possible vibrations depend on the molecular structure, such information may allow for determination of compounds existing in the sample or for quantification of their concentrations. Various modifications of this method, such as surface enhanced Raman spectroscopy or resonance Raman spectroscopy, can be used to increase intensity of scattering, although they have certain limitations, such as necessity to use certain materials or restriction of compounds which can be imagined with a certain laser wavelength. The largest problem is fluorescence of probed molecules and tissue, which often can overwhelm relatively weak Raman signal. Certain techniques, such as coherent anti-Stokes Raman scattering (CARS), can be used to remove the interference of fluorescence, though they require more sophisticated equipment and are more difficult to use (Auner et al., 2018).

One example of the application of Raman spectroscopy in brain tumor investigations is the work done by Galli and colleagues. They combined Raman and fluorescence spectroscopies to investigate brain tumor biopsies intraoperatively. Comparing with later histopathological studies, a correct classification ranging from 81 % for certain types of oligodendrogliomas and astrocytomas to 94 % for glioblastoma tumors was achieved (Galli et al., 2019). Modifications of Raman spectroscopy are used as well, as illustrated by research conducted by Le et al., who used two-photon spectroscopy together with CARS. In this case, CARS allowed them to detect reduced myelin concentrations in tumor sites. Although the system was more suitable for extraoperative use, it has some potential for intraoperative use, too, if several problems (small field of view and imaging depth) are overcome (Fig. 1.3.) (Le et al., 2017).

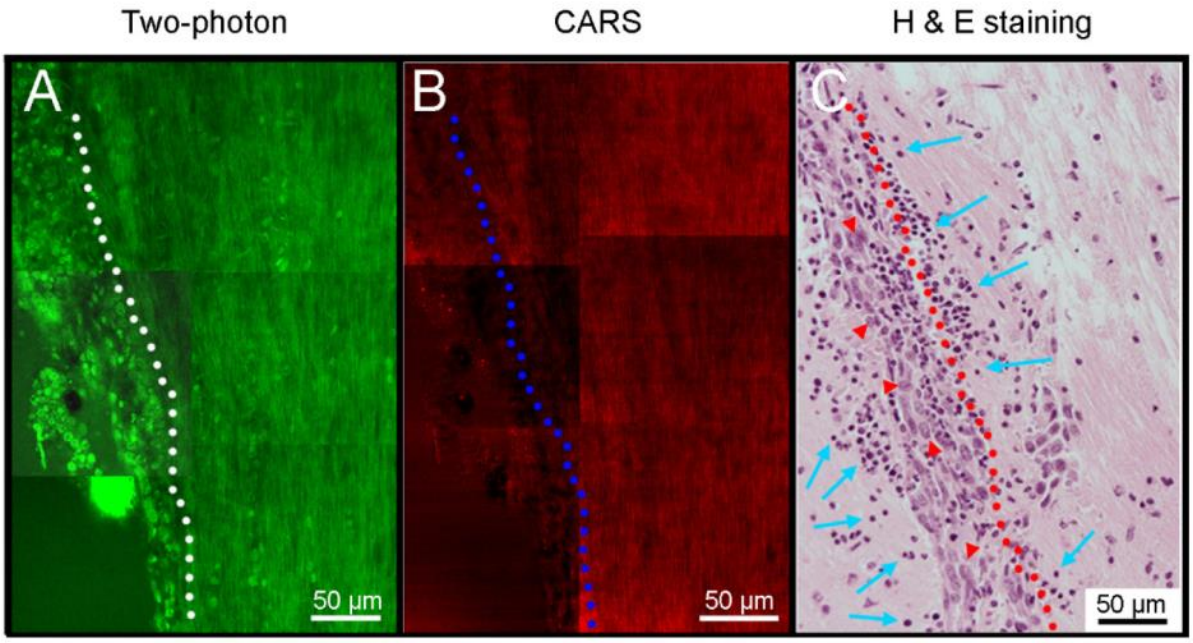

Figure 1.3. Images of the vicinity of a metastatic brain tumor: a) two-photon fluorescence spectroscopy image; b) CARS image; c) H & E stained tissue image (Le et al., 2017).

1.2.1.4. Optical coherence tomography

Optical coherence tomography (OCT) is an optical technique which uses differences in refractive index and light scattering properties of tissues to produce two-dimensional or three-dimensional images. Although OCT is mostly used in investigations of weakly scattering media, it can also be applied to image non-transparent media up to a few millimeters in depth. Its main advantages include high resolution and the ability to image intraoperatively (Wang et al., 2017).

Application of this method for both diagnostics and therapy is demonstrated by the research of Kut and colleagues, where they first used OCT to differentiate cancerous and non-cancerous tissue in human samples *ex vivo*, and after that tested the method intraoperatively in a murine model. It was possible to differentiate tumors *in vivo*, too, and researchers believe that the method has potential for future clinical use (Kut et al., 2015).

1.2.2. Application of optical methods for nervous system cancer therapy

1.2.2.1. Photodynamic therapy

Photodynamic therapy (PDT) is a method for treating some forms of cancer which involves the use of certain chemical compounds called photosensitizers (PSs). Working

principle of PDT is based on the generation of reactive singlet oxygen by a photochemical reaction involving PS (Fig. 1.4.). For the reaction to happen, PS molecules have to be excited by illuminating them with light of a proper wavelength (coinciding with absorption band of PS). There are two outcomes of excitation. First, a molecule can get excited to its singlet state. After this transition the molecule can return to the ground state by radiationless decay or by emission of a fluorescence photon. This fluorescence can be used to track the PS distribution in the body and to determine its distribution, which allows to ascertain whether PS is accumulated in the tumor being treated. Second possibility is the molecule's excitation to its triplet state. PS molecules in triplet state are reactive and can interact with other molecules in their surroundings. Two types of such reactions are distinguished. Type 2 reactions are the main reactions responsible for the effect of PDT. They result in generation of singlet oxygen, which is the main agent involved in destruction of cancerous cells. Type 1 reactions involve PS molecules interacting with various other compounds. These reactions result in generation of free radicals, including peroxide or hydroxyl radicals, which also can damage cancer cells (Patrice, 2004).

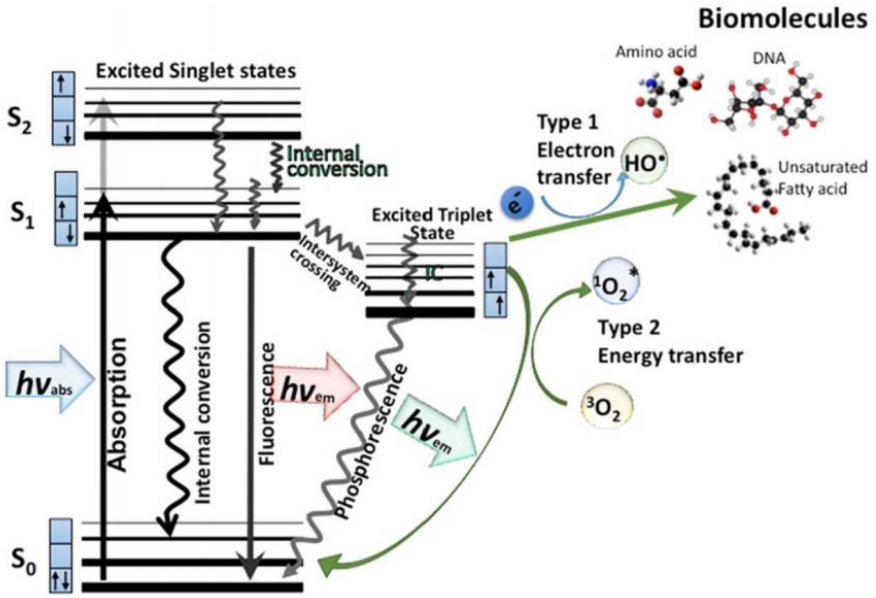

Figure 1.4 Jablonski diagram showing the mechanism of singlet oxygen generation in PDT (Abrahamse and Hamblin, 2016).

An important property of PDT is its selectivity for cancerous cells. Because of selective accumulation and retention, after some time PS's concentration in tumor will be higher than in the surrounding tissue (Castano et al., 2005). Selectivity, together with localized illumination of the tumor, allows to minimize damage to healthy cells, as generation of singlet oxygen will only take place in the illuminated body area. As PS itself is nontoxic,

this is an important advantage over conventional chemotherapy drugs. Other advantages include low cost, possibility of repeating the treatment procedure without substantial side effects and destruction of tumor vasculature together with cancer cells, thus increasing the effectiveness of treatment (Allison and Moghissi, 2013; Calixto et al., 2016).

Although PDT is mainly used for treatment of skin, neck and some other types of cancer, there is a growing tendency to apply this method for other cancers as well, including brain cancer. There are quite a few clinical trials investigating this application of PDT (Quirk et al., 2015), and in 2013 in Japan PDT has been approved as a treatment method for malignant brain tumors (Akimoto, 2016).

1.2.2.2. Photothermal therapy

Photothermal therapy (PTT) is a therapeutic method related to PDT. Both methods utilize light to illuminate light sensitive compounds, the main difference being the subsequent processes involved – while reactive oxygen species are being generated in the case of PDT, the therapeutic effect of PTT comes from heat being released from the excited molecules. In principle, tumors could be heated even without using any additional compounds, but that might result in damage to surrounding healthy tissue, as temperatures required are quite high (40 °C – 50 °C). Photothermal absorbers (indocyanine green dye, for example), which can be targeted to tumors, allow to reduce the excitation required to reach this temperature and to limit the damage to non-cancerous tissue (Doughty et al., 2019). PTT has mainly the same advantages as PDT and is investigated as a potential treatment strategy for metastatic cancer (Zou et al., 2016).

1.2.3. Drawbacks of optical diagnostic and therapeutic methods

Even though optical methods do have many advantages over other imaging techniques, they do have some drawbacks, the biggest being the shortcomings of optical probes. The majority of currently used probes are organic fluorescent dyes. Despite their use in medical imaging for quite some time, organic dyes have severe disadvantages, ranging from having small Stokes shift and low quantum yield to having low stability in tissue, high clearance rate or even causing toxic side effects. This complicates the acquisition of images by decreasing their quality and limiting the duration of imaging. Probably the biggest drawback is the lack of probes with good optical properties having absorption and emission peaks coinciding with

tissue absorption window, which severely limits the possible imaging depth (Fig. 1.5.) (McHugh et al., 2018). For brain tumor imaging in particular, one more serious drawback exists – organic dyes cannot cross the BBB. This hinders attempts to image brain tumors, at least until BBB is broken due to progressing cancer (Diaz et al., 2015).

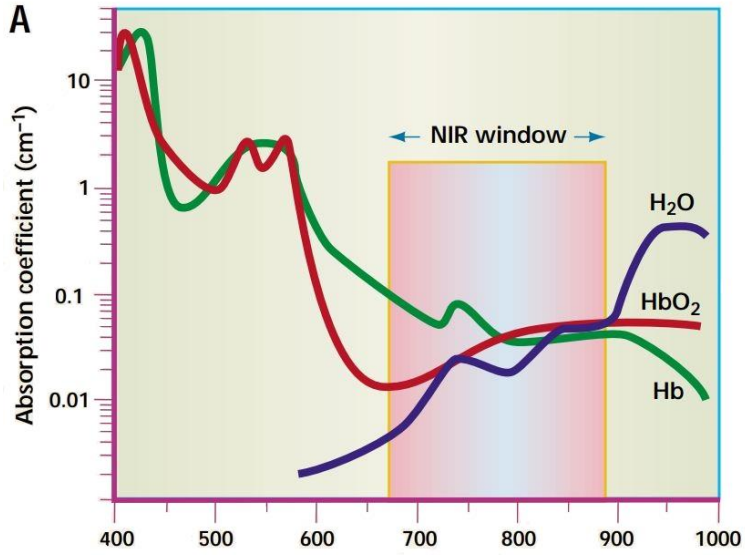

Figure 1.5. Dependence of extinction coefficient on wavelength in tissue and first tissue transparency window (Weissleder, 2001).

As is with diagnostic methods, optical therapeutic methods also have some drawbacks which keep them from gaining a more widespread acceptance in the medical community. In the case of PDT, even though PSs have some selectivity for cancer cells, it still takes large doses and long administration times for them to reach sufficient accumulation in tumors. This leads to significant PS concentrations in healthy cells, which can cause damage to healthy tissue during treatment procedure, as well as result in light sensitivity of skin for some time after treatment (Lucky et al., 2015). Another problem faced by clinicians working with PDT is illumination of the accumulated PS in tumors. Light used for illumination has to be absorbed as intensely as possible for efficient generation of singlet oxygen to occur. Maximum extinction coefficient of most PSs is for visible light in 400 nm – 600 nm interval (Fig. 1.5.). Tissue absorbs light of this interval as well and this makes it difficult to use PDT to treat tumors which are deeper than a few millimeters beneath the skin (Lucky et al., 2015). Although there are some PSs (namely bacteriochlorins) which absorb light of about 750 nm, which coincides with the tissue transmission window, they are still not used clinically, so absorption of light used for illumination is still an important disadvantage of PDT (Abrahamse and Hamblin, 2016). In addition, most of PSs are hydrophobic and aggregate in

aqueous solutions. This makes it difficult to use them clinically as it complicates the preparation of medication and causes only a part of such PS to reach its destination (Liu et al., 2017; Lucky et al., 2015). Dyes used for PTT have some faults as well – most widely used indocyanine-type dyes are quite unstable in biological environments and are quickly removed from the circulation, though, compared with PSs, they efficiently absorb light of 800 nm, coinciding with tissue absorption window. Their specificity for cancer cells could also use some improvement (Li et al., 2020). Most PSs and dyes used for PTT also have trouble bypassing the BBB, which limits their application for brain tumor treatment.

1.3. Use of nanomaterials in medicine

1.3.1. Nanomaterials

Because of their distinct properties differing from bulk materials, nanomaterials have found a variety of applications in medicine, most commonly as drug delivery or imaging agents. Nanomaterials, such as liposomes or various nanoparticles (NPs), can be functionalized, allowing to target them to the specified area, thus reducing the required amount of drug and minimizing damage to healthy tissue (Sharma, 2017). Imaging applications can also take advantage of functionalization. In addition, certain nanomaterials are more efficient imaging agents than commonly used organic dyes, featuring brighter photoluminescence and superior resistance to photobleaching (Smith and Gambhir, 2017). Taking into account the mentioned drawbacks of optical cancer imaging and treatment methods, nanomaterials may seem as a feasible solution to these problems.

1.3.2. Metallic nanoparticles

Metallic NPs include gold, silver and iron NPs, among others. Properties of metallic NPs depend on their composition – ones made from noble metals exhibit surface plasmon resonance phenomenon, which results in intense absorption at specific wavelengths, while iron NPs are magnetic (Patra et al., 2018). This can be useful in certain diagnostical applications – for example, noble metal NPs can be used for surface enhanced Raman scattering. Gold nanorods also absorb NIR light, making them useful in photothermal therapy (Moskovits, 2005). Metallic NPs are generally easily functionalized, which can be used for drug delivery or to increase their specificity (Patra et al., 2018).

Although metallic NPs are investigated for application in oncology, one example being gold NPs functionalized with doxorubicin and gadolinium contrast agents for theranostic application in glioma treatment (Cheng et al., 2014), due to their inadequately investigated nanotoxicity, other NPs, such as biodegradable organic NPs, are seen as more attractive alternatives (Zottel et al., 2019).

1.3.3. Biodegradable nanoparticles

Biodegradable NPs allow to avoid the main drawback of inorganic NPs – their accumulation, long term effects of which are not fully understood. Such NPs are synthesized from either synthetic (for example, polyactic acid) or natural (chitosan, among others) compounds. Over time, they break down into other non-toxic compounds, which are removed from organism (Su and Kang, 2020).

Two types of organic NPs are nanocapsules (micelles and liposomes) and nanospheres (dendrimers). Micelles are spheres of self-assembled amphiphilic molecules. Their center is hydrophobic, so they can be used to transport poorly soluble compounds. Liposomes are similar to micelles, the difference being that they are composed of a double layer of phospholipids, similar to a plasma membrane. Liposomes can carry higher loads of drugs and have a longer circulation lifetime, but their synthesis is more complicated, thus limiting their use. Dendrimers are, in simplest terms, branched molecules, which can be extensively modified due to having various functional groups. They have large drug carrying capacity because of their large surface area. Dendrimers are synthesized from various polymers, the most common being polyamidoamine (Su and Kang, 2020).

Various biodegradable NPs are investigated for their application in oncology, therapy of brain cancer included. One of the main advantages of such NPs in this area is their ability to pass the BBB. This was demonstrated in one recent study using liposomes loaded with doxorubicin and iron oxide NPs. These NPs were used to trigger drug release by applying an alternating magnetic field. Liposomes were also functionalized with antibodies against glioma cells to aid targeted delivery of drugs and a glioma cell-penetrating peptide, which reduced damage to noncancerous cells (Shi et al., 2019). In another experiment, MRI contrast agents together with a fluorescent dye were attached to dendrimers to create a combined optical imaging-MRI platform. The resulting NPs were successfully tested in a rat glioma model (Fig. 1.6.) (Jayasundara and Ali, 2017).

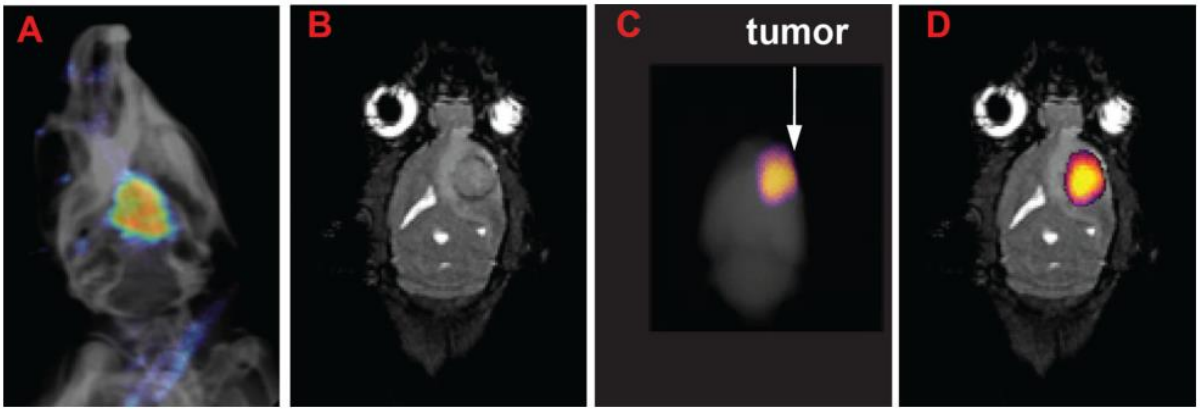

Figure 1.6. a) NPs localized in a rat brain tumor (overlay of a *in vivo* fluorescence and a X-ray image); b) MRI image; c) *ex vivo* fluorescence image of NPs localized in a rat brain tumor; d) overlay of b) and c) images (Jayasundara and Ali, 2017).

1.3.4. Carbon nanomaterials

Carbon-based nanomaterials include graphene, graphene QDs and carbon nanotubes (CNTs). These materials possess certain properties – high potential for functionalization, large surface area and high stability, which make them attractive for medical purposes. CNTs in particular are useful for drug delivery, where researchers are trying to encapsulate payload inside the nanotubes. This would allow for better control of drug release. CNTs also absorb NIR light and are suitable for PTT. Graphene, especially graphene oxide (GO), and graphene QDs have various functional groups, allowing for extensive functionalization and attachment of drug molecules (Maiti et al., 2019). GO can also be applied for PTT, as shown in research by Su et al., where they functionalized GO with porphyrin and tested this conjugate for PTT of glioma cells *in vitro* (Su et al., 2015). The main drawback of carbon nanomaterials is their toxicity, which severely limits their application in biomedicine (Maiti et al., 2019), although there are some results stating otherwise (Nurunnabi et al., 2013).

1.4. Quantum dots for nervous system cancer imaging and treatment

1.4.1. Quantum dots

QDs are semiconductor nanoparticles with diameters typically ranging from 2 nm to 10 nm. They are made from III-V (for example, InP or GaAs) and II-VI (CdSe and CdTe, probably the most popular materials for QDs) compound semiconductor materials and certain elemental semiconductors, like silicon and germanium. QDs are often synthetized with a shell

of another semiconducting material (one often used material for this purpose is ZnS), which serves to improve their optical properties compared with unshelled QDs. Furthermore, to improve their solubility in polar solvents, QDs are capped with a hydrophilic or amphiphilic polymer layer (Fig. 1.7.) (Yu et al., 2006).

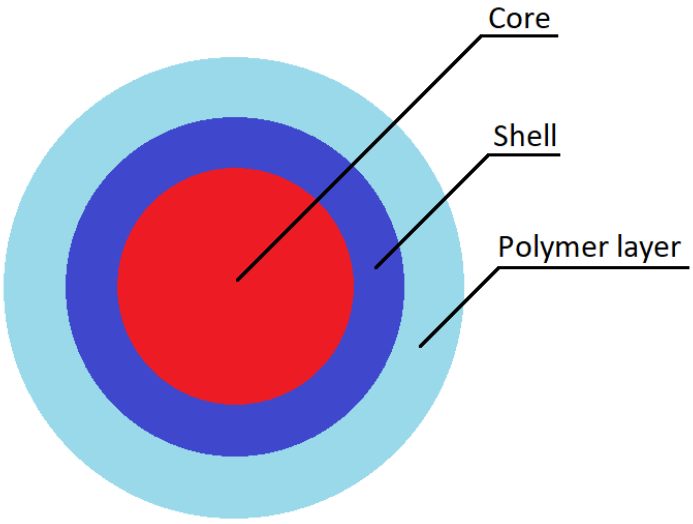

Figure 1.7. Schematic structure of a QD.

Methods of QD synthesis can be divided into two groups: bottom-up and top-down. Bottom-up methods include wet-chemical and vapor-phase methods. Wet-chemical methods use various chemical precursors to synthesize QDs in solution. Parameters such as temperature, pH and duration of the process influence the size of the synthesized QDs. Sol-gel and microemulsion processes are examples of wet-chemical methods. Vapor-phase synthesis is based on deposition of atoms on a substrate. QDs are formed due to lattice mismatch or differences in surface energies of substrate and deposited layer. Reactive species may also be used. Methods such as physical vapor deposition, metal-organic chemical vapor deposition and molecular beam epitaxy are vapor-phase methods (Bera et al., 2010). Bottom-up methods allow to synthesize large quantities of QDs in a short amount of time, but it can be difficult to control their size – separation techniques may be necessary to obtain QDs of a required size (Pranjal Vachaspati, 2013). Top-down methods are various lithography techniques, such as electron beam, ion beam or x-ray lithography. Although these methods allow to form uniformly sized QDs, they have some disadvantages, mainly long duration of process, possible contamination of formed QDs and structural deviations when patterning smaller QDs (Bera et al., 2010).

Unconventional optical and electronic properties of QDs arise because of their small size and high surface area to volume ratio and the resulting quantum confinement effect. When the size of a nanoparticle becomes less than the Bohr exciton radius of its material, energy levels of electrons become discrete, similar to an atom (Tartakovskiĭ, 2012). Another way to look at it is to compare QDs' size with de Broglie wavelength of its electrons – energy levels become quantized when QD is smaller than de Broglie wavelength (Fox, 2006). With most materials, diameter of less than 10 nm is enough for this to take effect. Quantum confinement is the reason of QDs' optical properties – high extinction coefficient, wide absorption and narrow photoluminescence (PL) spectra and high PL quantum yield (Yaghini et al., 2009). These optical properties and the possibility to tune them make QDs attractive for a wide range of applications, including medical imaging, where they are superior to traditionally used fluorescent dyes due to their longer lifetime, more intense PL and the ability to be functionalized with various biomolecules, which allows selective targeting of certain tissues (Marat Lutfullin and Osman M. Bakr).

1.4.2. Advantages of using quantum dots for cancer diagnostics and therapy

Use of QDs for imaging has numerous advantages over conventionally used imaging agents. As mentioned before, because of their intrinsic properties, QDs exhibit more intense fluorescence than organic fluorescent dyes, higher resistance to photobleaching and larger Stokes shift, all aiding in development of an efficient fluorescence platform. Due to their tunability, QDs emitting at various wavelengths can be synthetized, even at near infrared (700 nm – 900 nm), coinciding with tissue transparency window (Fig. 1.5.) (Blackman et al., 2008), which would allow to image tissue up to 1 cm in depth or even deeper. In addition, QDs can be extensively modified by functionalization, which can make them specific to tumors, thus improving image quality (Fang et al., 2012). In a more advanced application, they could even be used to image certain biomarkers and in this way elucidate the possible progression of the tumor (True and Gao, 2007). Certain QDs could be useful not only for optical imaging, but for other imaging types as well, such as MRI, what can lead to a development of a multimodal imaging method (Sheng et al., 2018). More importantly, QDs have some capacity to overcome the BBB, what is a major advantage over fluorescent dyes for brain tumor imaging. There is some research done investigating this property, such as using carbonized polymer QDs to image glioma tumors in rats, where such QDs were shown

to be able to penetrate the BBB, accurately localize in the tumor and fluoresce for a few hours at least (Fig. 1.8.) (Liu et al., 2018).

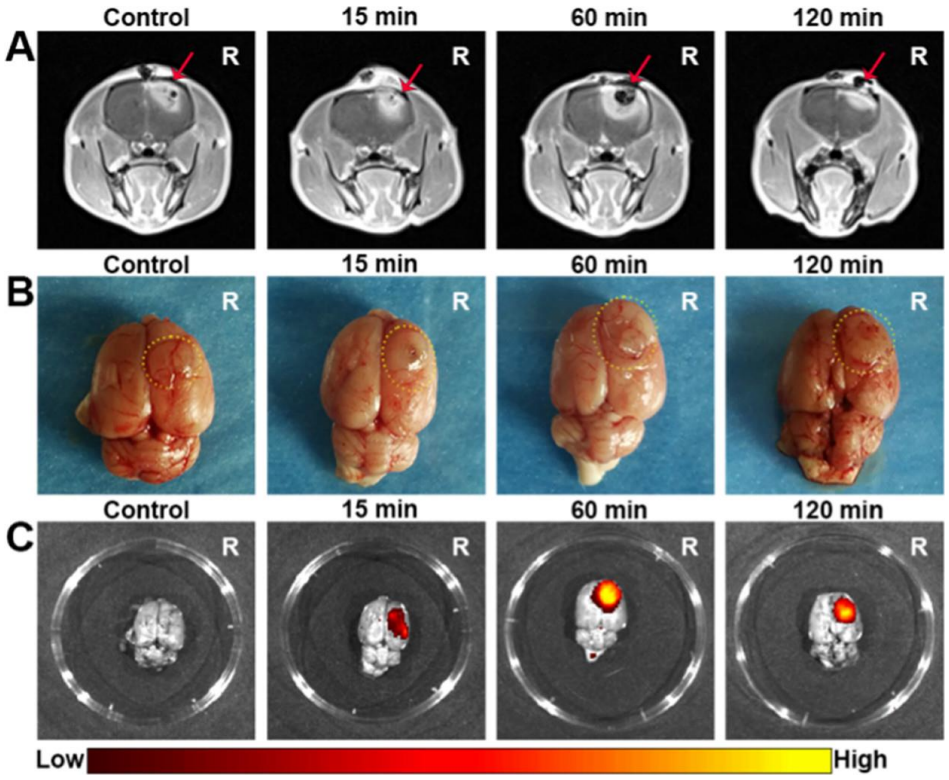

Figure 1.8. MR images of rat brains with glioma tumors (indicated by arrows) (A), photographs of dissected rat brains with glioma tumors (tumors are marked) (B) and *ex vivo* fluorescence images of rat brains with glioma tumors after injection of QDs in the tail vein, showing their capability of passing the BBB (C) (Liu et al., 2018).

As for imaging, QDs can also be used to circumvent some of the disadvantages of optical cancer therapeutic methods. For PDT, selectivity and hydrophilic properties of PSs can be enhanced by attaching PS molecules to nanoparticles (NPs) and forming PS–NP complexes. Being a type of NP, QDs are also suitable for making complexes with PSs (Fig. 1.9.). They can improve PS selectivity for tumors by preventing its premature release into healthy tissue or enhancing its permeability and retention in tumors, as well as increase PS hydrophilicity. QDs can also be functionalized to further improve selectivity (Lucky et al., 2015). Certain QDs exhibit two photon absorption or photon upconversion phenomena. Both of them make it possible to use light of longer wavelength for excitation of PS molecules, allowing to treat deeper tumors (Li et al., 2012). Förster resonance energy transfer (FRET) can also be used to the same effect by nonradiatively transferring energy from illuminated QDs to closely located PS molecules (Clapp et al., 2006). Also, intense PL of QDs can be

used to track distribution of complexes in the body during treatment procedure (Valanciunaite et al., 2010).

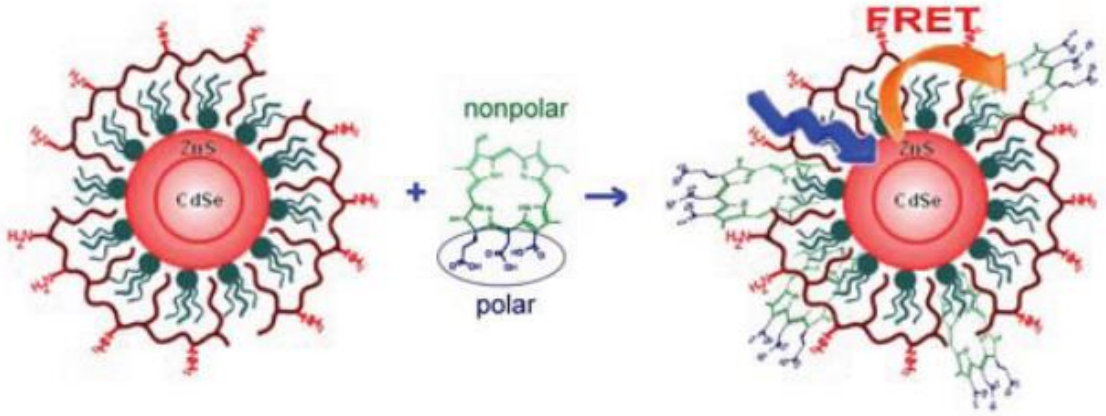

Figure 1.9. Scheme showing the formation of QD-Ce6 complex (Valanciunaite et al., 2010).

Nanomaterials are also being investigated for application in PTT as radiation absorbers. Although most of the research is on metal or graphene nanoparticles, there is some work done on QDs as well (Doughty et al., 2019). As with PDT, they can be used for more efficient targeting of tumors, in some cases even without any functionalization (Bao et al., 2018). Other than that, compared with dyes used for PTT, QDs are generally more stable and have good photothermal conversion efficiency (Wang et al., 2019). There is even research on using QDs to combine both PDT and PTT into one therapeutic platform, serving as a good example of their versatility (Zhang et al., 2018).

1.5. Nontoxic quantum dots

1.5.1. Nanotoxicity

Having read the preceding section it may seem that QDs are perfect imaging and therapeutic agents. Although they do have many attractive qualities, there are also some drawbacks of using QDs, namely nanotoxicity. As QDs and other NPs are sufficiently small, they can cross the plasma membrane or be endocytosed or phagocytosed and enter the inside of cells. There, over time, they can accumulate in organelles and possibly have some effect, such as influence generation of reactive oxygen species or cause genotoxicity. The effect may

come from QDs themselves or from their constituent chemical elements, which may be released during their degradation in cells (Ehrhart et al., 2015).

Cell death is not the only possible outcome of nanotoxicity – NPs may also influence cell activity and functioning in more subtle ways. Due to the sensitivity of the nervous system to such interferences, this could have some dangerous outcomes, so assessing nanotoxicity of QDs in neurons and their effects on neuronal properties is of the utmost importance for their application as NS cancer imaging and therapeutic agents. There is a series of articles by Zhaowei group investigating nanotoxicity of various NPs, which generally reports that they increase the excitability of neurons (Liu et al., 2009, 2012). This has been confirmed by Jung et al., who also investigated effects of NPs on seizure models and found that they may influence certain neurological disorders, such as epilepsy (Jung et al., 2014). It must be noted that these studies investigated other NPs, not QDs, so their effects may vary from those described. In any case, lack of information on neurotoxicity of QDs severely limits their possible application for NS cancer imaging and therapy.

1.5.2. Nontoxic $CuInS_2$ quantum dots

Disregarding the lack of studies on QD neurotoxicity, another reason limiting their medical application is well-known toxicity of commonly used QDs. The most investigated and widely used QDs, CdSe and CdTe, contain cadmium, which is a toxic heavy metal. Harmful effects of QDs on cell viability are widely investigated (Mo et al., 2017). This also restricts the application of other QDs with potential for clinical use, such as lead chalcogenide QDs (for example, PbS, PbSe and PbTe), which absorb and photoluminesce in the tissue transparency window (van Veggel, 2014). Both types of QDs exhibit good optical properties which would be suitable for imaging and therapeutic applications.

Not all QDs are made of toxic materials, though – there are some that do not contain heavy metals. One such material is $CuInS_2$ (CIS), and QDs composed of this material have been shown to be less toxic than conventional CdSe QDs (Fig. 1.10.) (Pons et al., 2010). In addition, they emit light in the NIR region, corresponding with tissue transparency window. This property, together with their biocompatibility and good optical properties (large Stokes shift, long PL lifetime and high quantum yield, which can be further increased by capping them with a ZnS shell), make CIS QDs ideal for clinical applications (Pons et al., 2010).

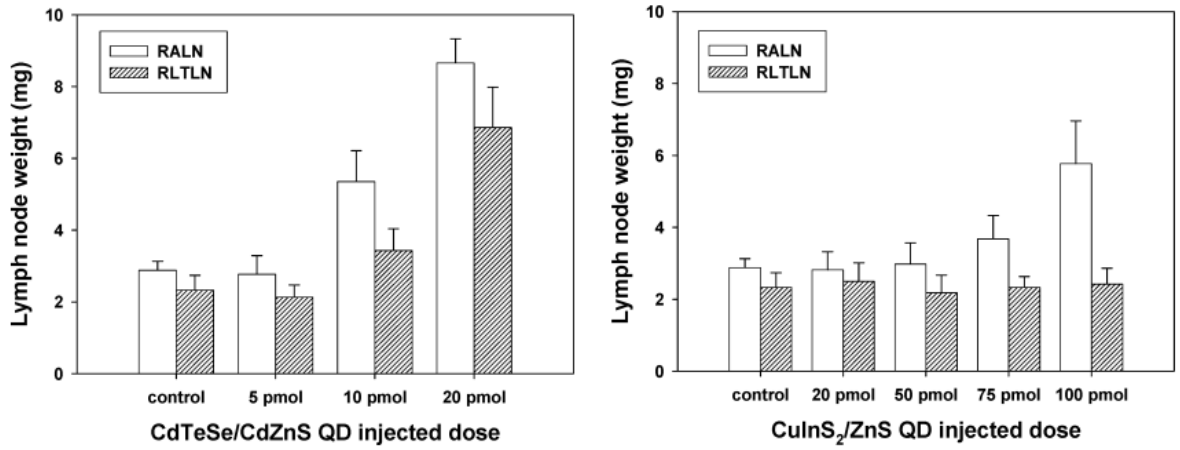

Figure 1.10. Weights of two rat lymph nodes after injections of different concentrations of Cd and $CuInS_2$ QDs (increase in weight is due to inflammation caused by nanotoxicity of QDs, RALN – right axillary lymph node, RLTLN – right lateral thoracic lymph node) (Pons et al., 2010).

1.5.3. $CuInS_2$ quantum dots for cancer imaging, photodynamic therapy and photothermal therapy

Although CIS QDs have been known for quite some time, there are not that many articles detailing research on their use for cancer theranostics. Even then, there exist some interesting examples of their application. Probably the most basic use of QDs involves functionalizing them in some way which should increase their specificity to certain tumors. Michalska et al. used a certain protein with specificity for HER2-positive cells (HER2 receptor overexpression is a known factor in breast cancer development) for selective fluorescent labelling of such cells with CIS/ZnS QDs (Michalska et al., 2016). Even though breast cancer cells were used in this study, HER2-positive breast cancer is known to metastasize and form secondary CNS tumors (Duchnowska et al., 2018), which in principle could also be imaged with these QD-protein conjugates. A more complex example of application of these QDs for imaging could be CIS QD/silica composite described by Foda et al. CIS/ZnS QDs were incorporated into silica beads by encapsulating them within silane micelles. This was found to increase the stability of QDs in aqueous media without negatively affecting their optical properties. Suitability of these composites for imaging was investigated using HeLa cervical cancer cells (Foda et al., 2014).

Even more advanced diagnostic applications might involve more than one imaging type at once. As an example of using CIS QDs in this way, a conjugate of Prussian Blue-coated magnetic Fe_3O_4 NPs, CIS/ZnS QDs and hyaluronic acid was described by Yang et al. Such conjugates could be used for optical imaging, as well as for enhancing MRI images.

Accumulation of conjugates in HeLa cells was found to be influenced by external magnetic field, showing that it might be used to localize NPs in the required body area. Even more, the use of conjugates for photothermal therapy *in vivo* was also investigated, and their effectiveness was shown, indicating the possible theranostic use of these NPs (Yang et al., 2017).

None of the above described experiments investigated the application of CIS QDs for imaging of NS cancer. Only one such study was found, in some ways similar to Yang's et al. work – researchers coupled CIS/ZnS with gadolinium for MRI enhancement and with CD133 antibody for cancer stem-like cell specificity. CD133 is a protein found in stem-like cells of some types of cancer, including gliomas. The effect of conjugates was investigated both *in vitro* using SU2 glioblastoma stem cell line and *in vivo* by imaging tumors inoculated in mice. Although QDs were found to accumulate at the tumor for up to 20 hours post injection, their accumulation in some other body parts, namely liver, may prove a hindrance in real applications of these nanomaterials. MRI enhancement, on the other hand, was seen to be better than with a commercial contrast agent, even with NPs without CD133 antibody (Fig. 1.11.) (Zhang et al., 2016).

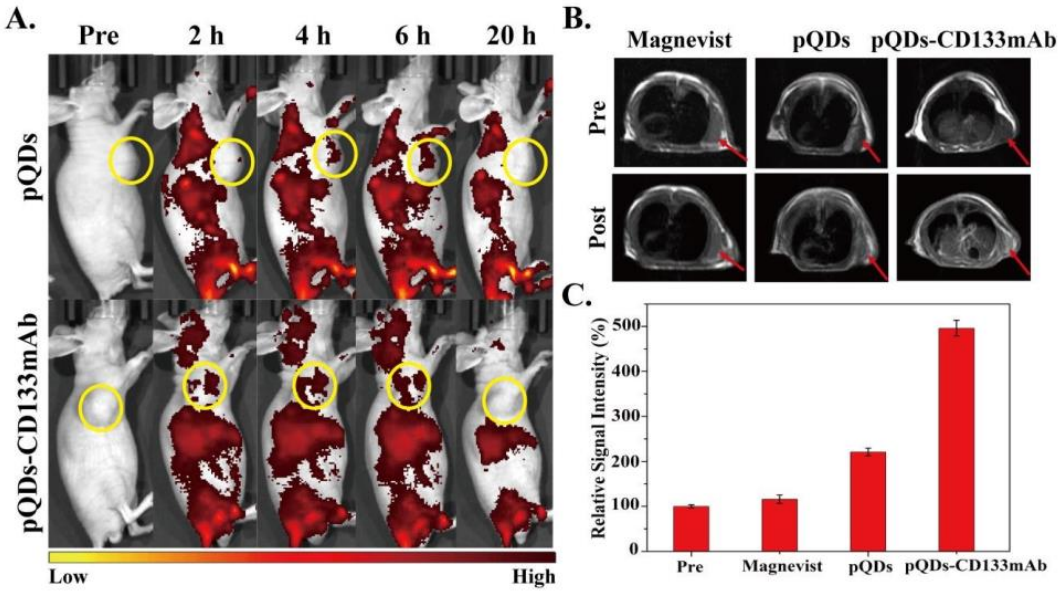

Figure 1.11. The accumulation of QDs without (top) and with CD133 antibody (bottom) in tumors (yellow circles) over time (A); MRI images of tumors using commercial Magnevist contrast agent, QDs without antibody and with CD133 antibody pre- (top) and post injection of imaging agent (bottom) (B); relative MR signal of used contrast agents (C) (Zhang et al., 2016).

The situation is similar with research on CIS QDs for PDT – no articles describing such use for nervous system cancer treatment were found, although there are some investigations on these QDs for PDT of other cancer types. Examples include synthesis of complexes of CIS QDs and certain porphyrins (Tsolekile et al., 2018) or 5-aminolevulinic acid (Feng et al., 2016). The effectiveness of the first complex was not investigated, while the second one was found to exhibit some cytotoxicity even when not illuminated, so the applicability of these complexes in clinical settings is questionable. Wu et al. report on CIS/ZnS QD and reduced graphene oxide composites. Role of graphene in this case was to lower the toxicity of these QDs even further, but it was found to also enhance other properties of QDs, such as accumulation in tumors or PL intensity. Complex was also found to be more effective in both *in vitro* and *in vivo* settings (Wu et al., 2016).

Same as with PDT, research on the application of CIS QDs for nervous system cancer PTT is nonexistent, but there are a few articles detailing their use for PTT of other cancers. Aside from the aforementioned Fe_3O_4 NP, CIS/ZnS QD and hyaluronic acid composites by Yang et al., there is one article describing using CIS/ZnS QDs for a combined PDT/PTT approach. Authors report that QDs inhibited growth of tumors in mice after phototreatment. In addition, they were also effective as imaging agents (Lv et al., 2016).

2. MATERIALS AND METHODS

2.1. Materials

Phosphate buffered saline (PBS), Dulbecco's modified Eagle's medium (DMEM), fetal bovine serum (FBS), penicillin/streptomycin (all from Thermo Fisher Scientific) and Hoechst 33258 dye (Sigma Aldrich) were used for cell culturing and experiments. Deionized water was produced with MicroPure UV water purification system. MDA-MB-231 (human breast cancer cell line) and U87 (human glioblastoma cell line) cells were acquired from ATCC. Amine-functionalized (aQDs) and carboxyl-functionalized (cQDs) CIS/ZnS core/shell QDs were synthesized at the Center of Energy, Materials and Telecommunications, University of Quebec, Canada.

2.2. Methods

Absorbance measurements

Absorption spectra of CIS/ZnS QDs were measured using Varian Cary 50 UV-Vis spectrophotometer. QD solution in deionized water (0,6 μg/ml concentration for aQDs and 1,6 μg/ml for cQDs) was used for the measurements. Quartz cuvettes of 1 cm optical path length were used. Spectra were measured over 250 nm – 850 nm wavelength interval with a step size of 1 nm and integration time of 0,1 s.

Photoluminescence measurements

PL spectra of CIS/ZnS QDs were acquired using Edinburgh Instruments FLS980 fluorescence spectrometer. QD solution in deionized water (0,8 μg/ml concentration for all types of QDs) was used for the measurements. Standard plastic cuvettes of 1 cm optical path length were used. Light of 550 nm from xenon lamp was used for excitation. Excitation and emission slit widths both were 7 nm and 12 nm, respectively. PL spectra in the range of 570 nm – 850 nm were collected with a step size of 1 nm and integration time of 0,1 s.

Dynamic light scattering and zeta potential measurements

Dynamic light scattering (DLS) and zeta potential measurements were performed on CIS/ZnS QD solutions in deionized water (0,6 μg/ml concentration for aQDs and 1,6 μg/ml for cQDs) using Brookhaven ZetaPALS zeta potential analyzer. Distribution of hydrodynamic diameters of QDs was determined from 10 consecutive DLS measurements. Zeta potential was determined after 10 measurements consisting of 10 cycles each. Before zeta potential measurements electrode was conditioned using saline solution (30 measurements of 10 cycles each).

Atomic force microscopy measurements

Morphology of CIS/ZnS QDs was investigated using Veeco diInnova atomic force microscope. CIS QDs were deposited on freshly cleaved mica surface by drop casting 10 μl of 1,6 μl/ml QD solution. Tapping mode was used for the measurements. Silicon cantilevers (Veeco) with tip radii < 10 nm and resonance frequency of 244 kHz – 295 kHz were used. Scanning rate was 1 Hz, image size – 5 μm × 5 μm. Images were processed (plane correction, leveling, Z-scale correction) using Gwyddion 2.53 software.

Investigation of quantum dot photoluminescence stability

CIS/ZnS QD solutions in PBS and DMEM (QD concentration 0,8 μg/ml in both solutions for all types of QDs) were prepared in standard plastic cuvettes of 1 cm optical path length. Cuvettes were sealed with Parafilm to prevent solvent evaporation. Blank samples of PBS and DMEM without QDs were prepared as well. PL and fluorescence lifetime (FL) spectra were registered every 24 hours over a one-week period using Edinburgh Instruments FLS980 fluorescence spectrometer. For PL measurements, xenon lamp was used for illumination of the sample. Light of 550 nm was used for excitation to reduce fluorescence of DMEM. Excitation and emission slit widths were equal to 7 nm and 12 nm, respectively. PL spectra in the range of 570 nm – 850 nm were collected with a step size of 1 nm and integration time of 0,1 s. For FL measurements, a 405 nm laser diode with tunable pulse frequency was used for excitation of fluorescence. Wavelengths coinciding with PL peaks of QDs were selected as emission wavelengths. Emission slit width was 15 nm. Emission count rate was kept at below 10 % of excitation count rate value to avoid photon pileup effect. Peak

value of 1000 counts was used as the stop condition. Spectra were baseline corrected by subtraction of the PL spectrum of respective solvent (PBS or DMEM). FL spectra were fitted with an exponential fit (reconvolution method) and analyzed using FAST 3.1 software.

Growth of cell cultures

Both MDA-MB-231 and U87 cell lines were grown in 25 cm^2 flasks in media consisting of DMEM supplemented with 10 % FBS (v/v) and penicillin (100 U/ml)/streptomycin (100 mg/ml) (P/S) at 37 °C in atmosphere containing 5 % CO_2.

Incubation of cells with quantum dots

U87 cells were seeded in an 8 well plate (Lab Tek Chambered Coverglass, Thermo Fisher Scientific) (25000 cells per well). DMEM / 10 % FBS / 1 % P/S was used as cell medium (400 µl per well). Cells were kept at 37 °C with 5 % CO_2. 24, 6, 3 and 1 hour prior to imaging cell medium in corresponding pairs of wells was changed to 225 µl DMEM / 10 % FBS / 1 % P/S in one well and DMEM / 1 % P/S in the second well (Fig. 2.1.). Solution of CIS/ZnS QDs was added to each well to a total volume of 250 µl in each well, producing QD concentration of 16 µg/ml. During incubation, plate was kept at 37 °C at 5 % CO_2. After the completion of incubation, medium with QDs was aspirated, cells were thrice washed with PBS and medium was changed to DMEM / 10 % FBS / 1 % P/S or DMEM / 1 % P/S (both with Hoechst dye (25 µg/ml)) in respective wells and kept for 30 minutes. After incubation with Hoechst dye, medium was aspirated, cells were thrice washed with PBS, medium was changed to DMEM / 10 % FBS / 1 % P/S or DMEM / 1 % P/S and cells were imaged using confocal microscopy.

24 h +FBS	6 h +FBS	3 h +FBS	1 h +FBS
24 h -FBS	6 h -FBS	3 h -FBS	1 h -FBS

Figure 2.1. Schematic representation of an 8 well plate used in the experiment.

Investigation of quantum dot accumulation in cells

After incubation with QDs live cells were imaged using Nikon Eclipse Te2000-U C1 Plus confocal scanning microscope. A Nikon Plan Apo VC 60× 1,4 NA immersion objective was used for imaging. 405 nm diode laser was used for excitation of both Hoechst dye and QDs. Fluorescence from Hoechst and QDs was collected using 450/17 nm and 605/35 nm band pass filters, respectively. Both channels were recorded separately to avoid spectral overlapping. Brightfield images were acquired as well. Images were analyzed using Nikon EZ-C1 3.90 software.

Cell viability assessment

Cell viability after incubation with QDs was determined using XTT cell viability assay. U87 cells were seeded in a 96 plate well with a density of 20000 cells per well and grown in 150 µl of DMEM / 10 % FBS / 1 % P/S medium. Effect on cell viability of 3 factors – concentration of QDs (16 µg/ml and 20 µg/ml), type of media (complete and serum-free) and incubation time (24 h and 48 h) – was investigated. Cells were incubated in 125 µl of media with QDs, while control cells were incubated in the same volume of medium without QDs. After incubation, medium with QDs was changed to medium consisting of 66,7 % of [DMEM / 10 % FBS / 1 % P/S], 32,6 % XTT and 0,67 % XTT activator. Cells were incubated for 3 more hours, after which light absorption measurements were performed with a plate reader. Optical density was measured at 490 nm (XTT absorption) and 630 nm (nonspecific absorption). Measured optical densities were corrected for nonspecific absorption and absorption due to media. Cell viabilities were determined by comparing optical densities of specific wells with control wells. Two-sample t-tests were used to compare samples for statistical significance.

3. RESULTS

3.1. Characterization of quantum dots

Normalized absorption spectra of aQDs and cQDs are shown in Fig. 3.1. PL spectra of the same QDs are shown in Fig. 3.2. AFM images and DLS histograms of QDs are shown in Fig. 3.3.

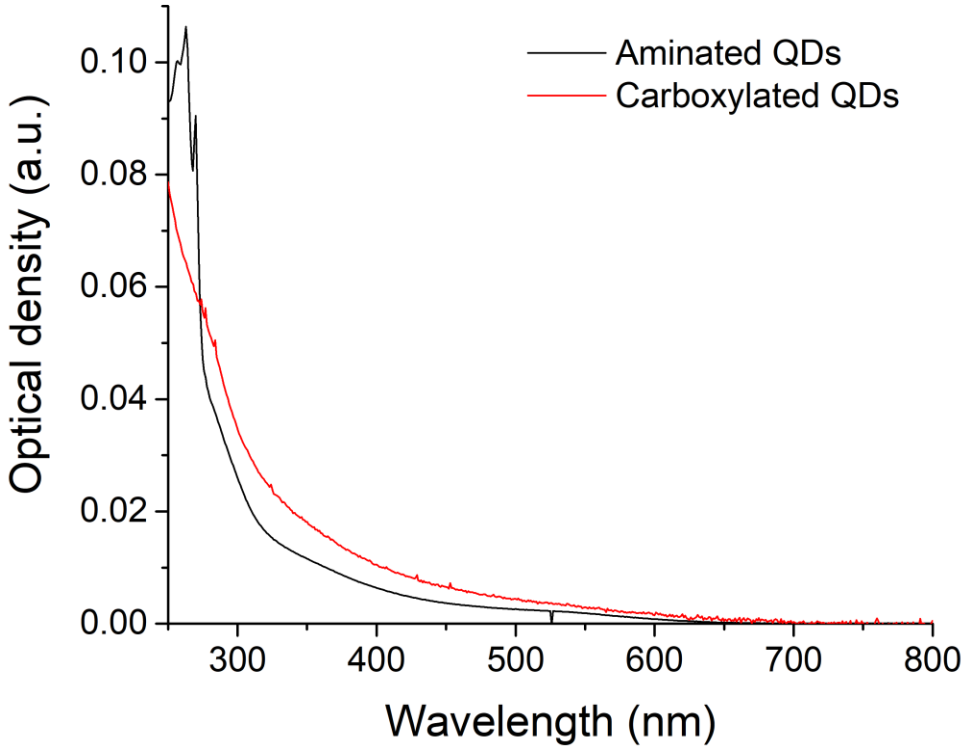

Figure 3.1. Normalized absorption spectra of aQDs and cQDs in deionized water (aQD concentration 0,6 µg/ml, cQD concentration 1,6 µg/ml).

Absorption of all types of QDs decreases going from UV to NIR region. Spectrum of cQDs is blue shifted compared with aQDs.

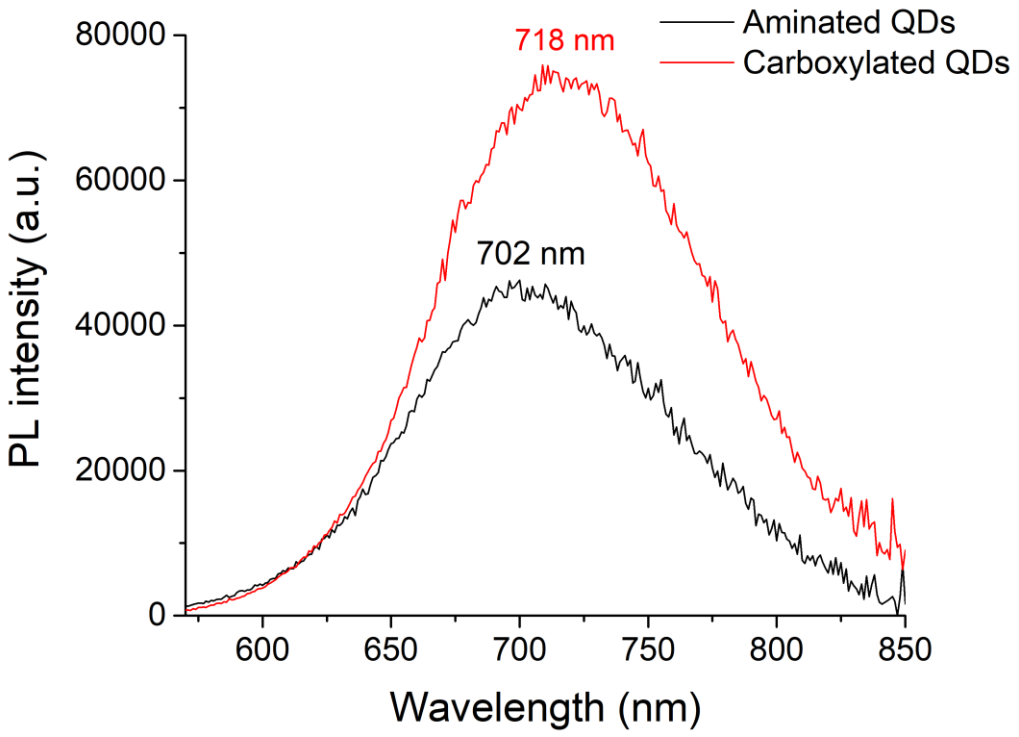

Figure 3.2. PL spectra of aQDs and cQDs in deionized water (concentration 0,8 μg/ml for both types of QDs).

PL spectra of aQDs and cQDs are centered at 702 nm and 718 nm, respectively, and they both range from about 550 nm to 850 nm. PL of cQDs is about 2 times more intense than PL of aQDs.

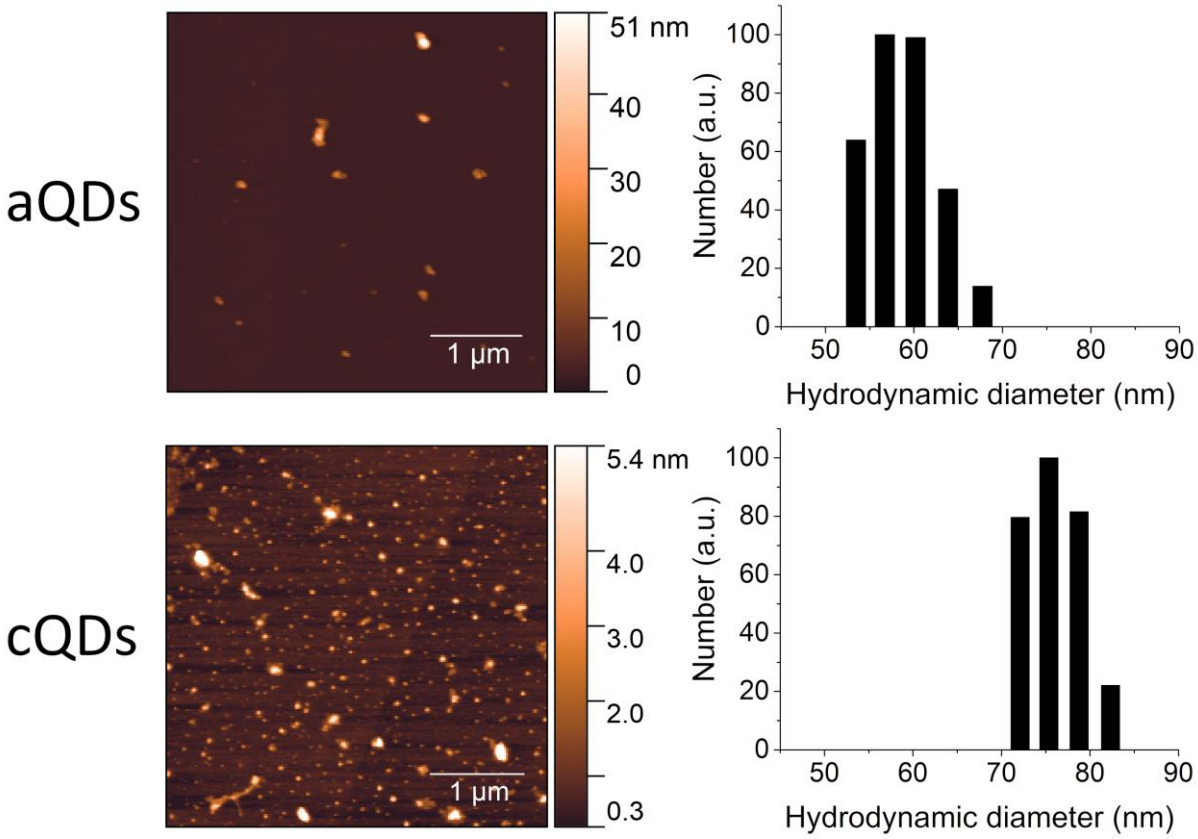

Figure 3.3. AFM images and DLS histograms of aQDs and cQDs.

Average size of aQDs is 6,6 nm ± 2,3 nm, while their average hydrodynamic diameter is 58,6 nm and zeta potential is -5,3 ± 0,3 mV. Average size of cQDs is 2,8 nm ± 0,9 nm, their average hydrodynamic diameter is 76 nm and zeta potential is -41,6 ± 1,9 mV.

3.2. Stability of quantum dots

PL spectra measured every 24 hours over a period of one week, as well as FL decay curves and DLS histograms at the beginning of the stability test and after one week, are presented in Figs. 3.4. and 3.5. (aQDs in PBS and DMEM media) and Figs. 3.6. and 3.7. (cQDs in PBS and DMEM media).

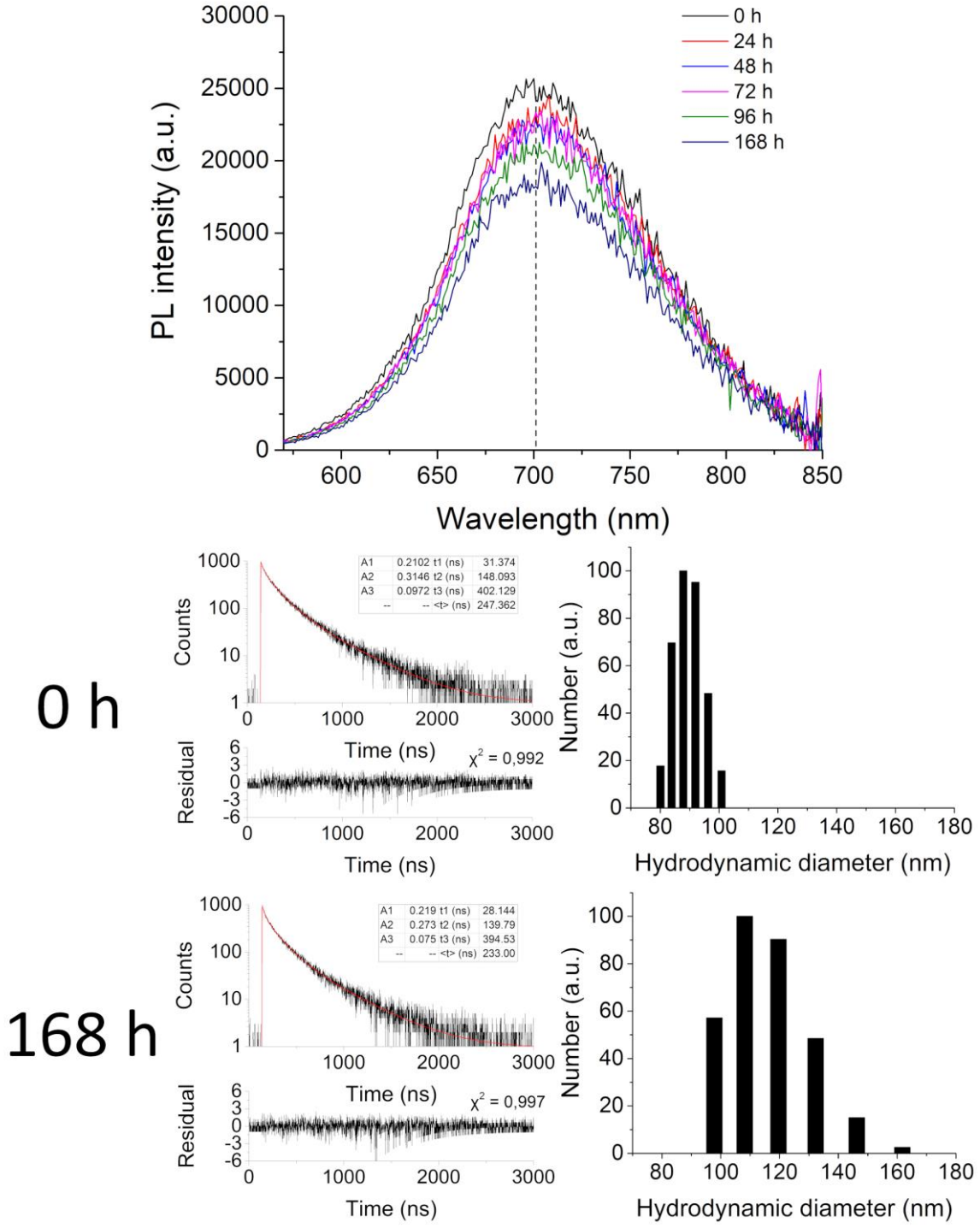

Figure 3.4. PL spectra of aQDs in PBS measured every 24 hours over a period of one week, as well as FL decay curves and DLS histograms at the beginning of the experiment and after one week. FL decay curves were fitted using a sum of 3 exponential functions, residuals and χ^2 values are presented.

During the week, PL intensity of aQDs in PBS decreased by about 26 % and average FL lifetime decreased by about 6 %. Average hydrodynamic diameter increased from 90 nm to 116 nm (about 29 % increase).

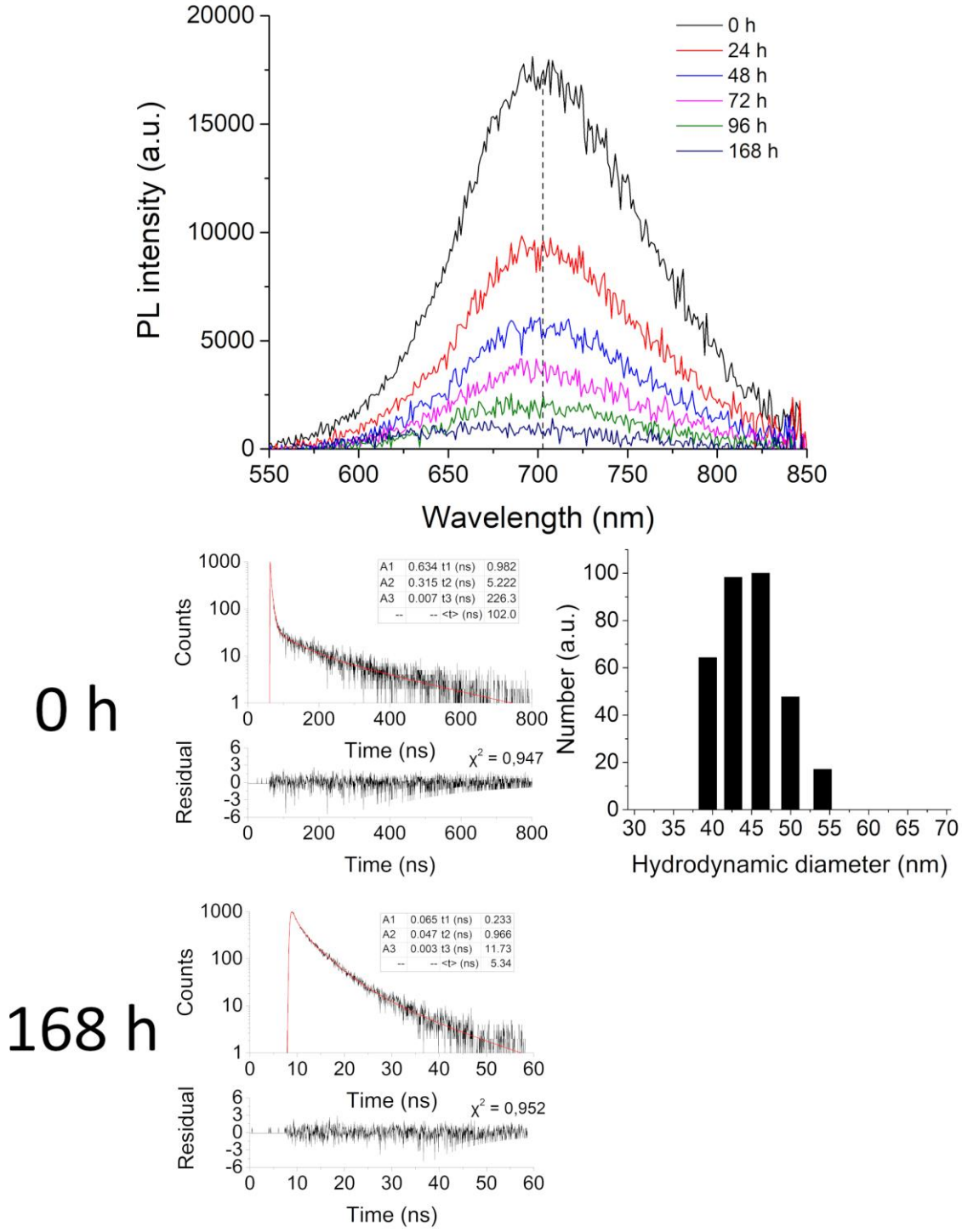

Figure 3.5. PL spectra of aQDs in DMEM measured every 24 hours over a period of one week, as well as FL decay curves and DLS histograms at the beginning of the experiment and after one week. FL decay curves were fitted using a sum of 3 exponential functions, residuals and χ^2 values are presented. DLS histogram at 168 h could not be properly measured.

During the week, PL intensity of aQDs in DMEM decreased by about 95 % and average FL lifetime also decreased by about 95 %. Average hydrodynamic diameter was 45 nm; it was not possible to measure it at the end of the experiment.

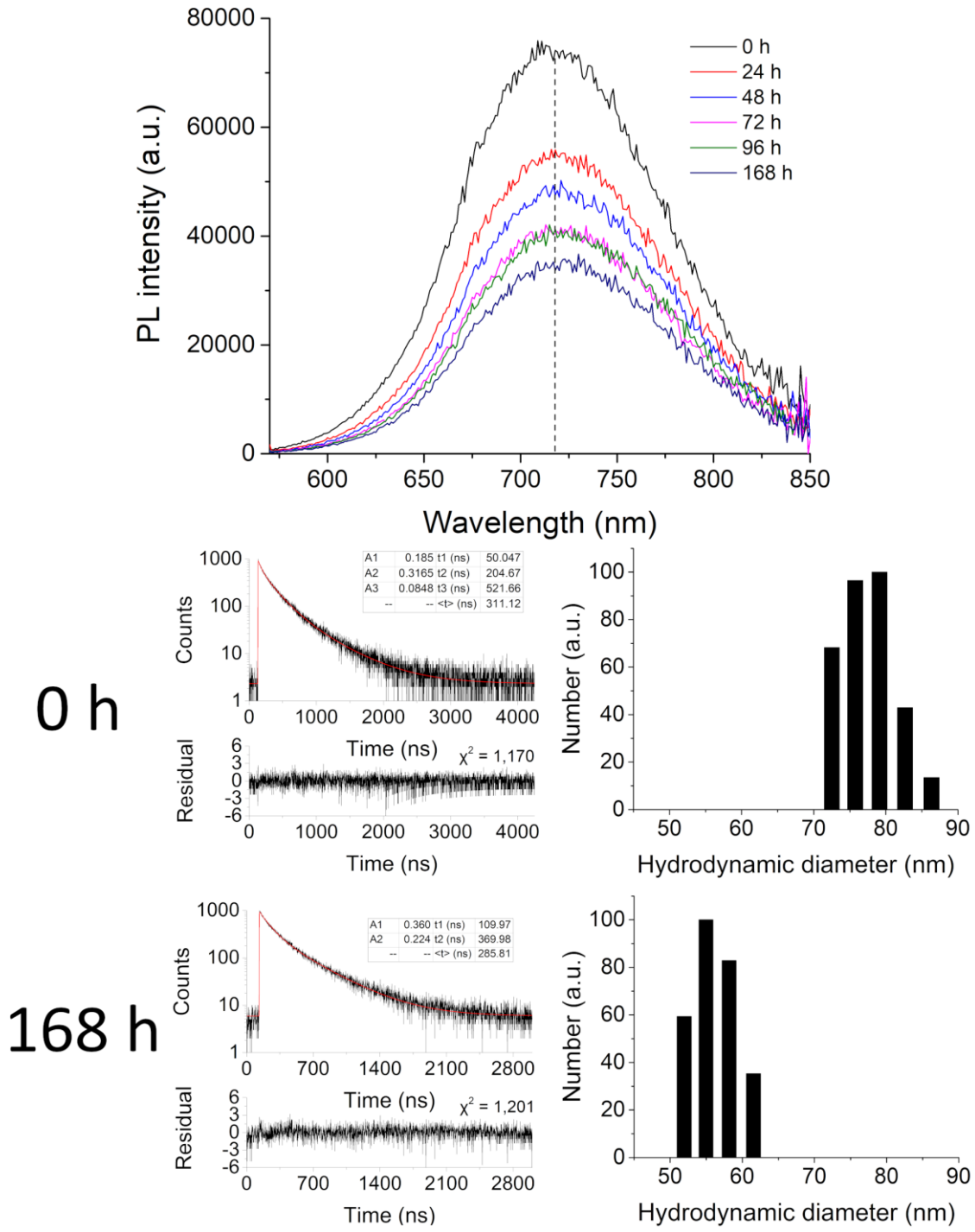

Figure 3.6. PL spectra of cQDs in PBS measured every 24 hours over a period of one week, as well as FL decay curves and DLS histograms at the beginning of the experiment and after one week. FL decay curves were fitted using a sum of 3 (at 0 h) or 2 (at 168 h) exponential functions, residuals and χ^2 values are presented.

During the week, PL intensity of cQDs in PBS decreased by about 53 % and average FL lifetime decreased by about 8 %. Average hydrodynamic diameter decreased from 77 nm to 56 nm (about 27 % decrease).

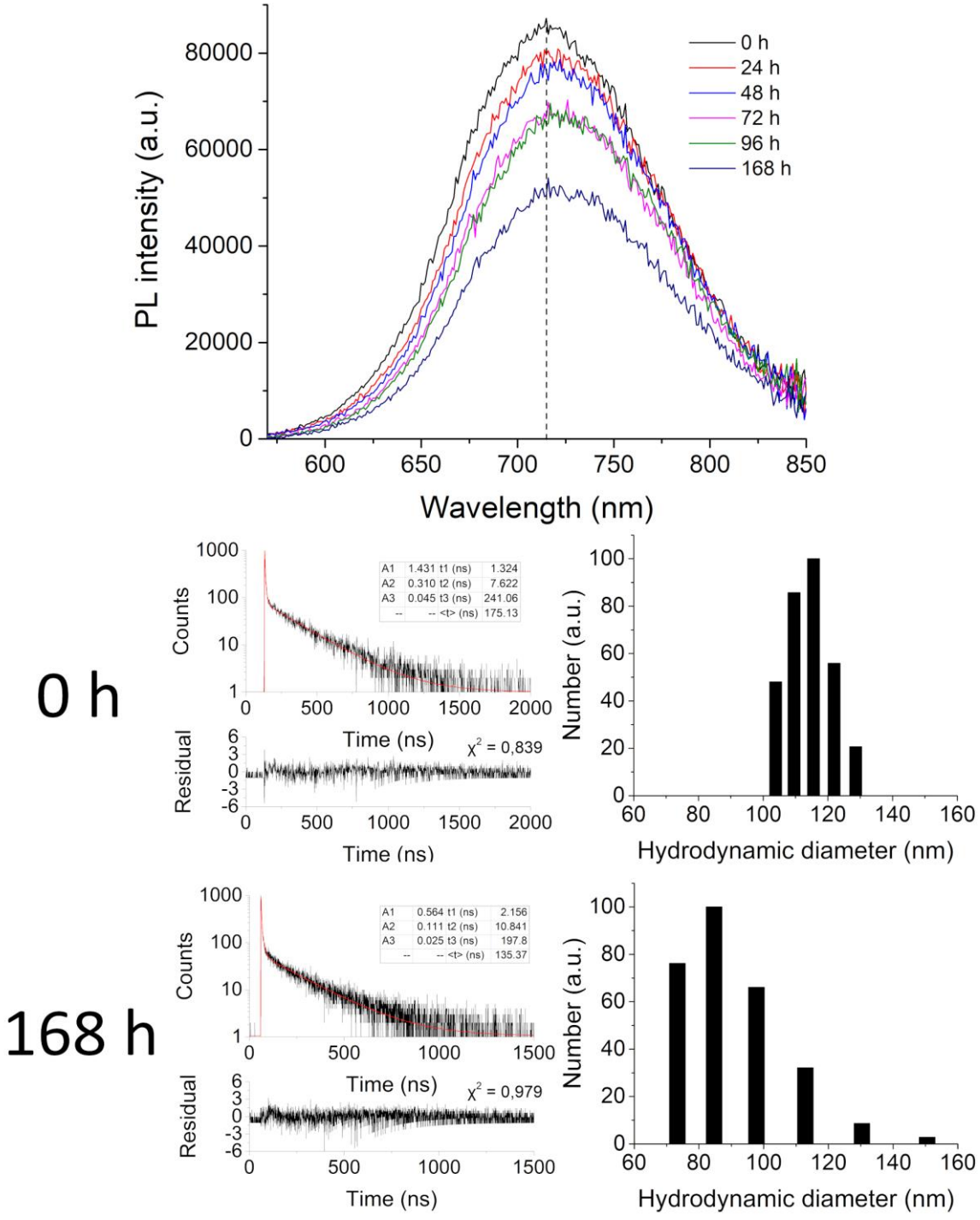

Figure 3.7. PL spectra of cQDs in DMEM measured every 24 hours over a period of one week, as well as FL decay curves and DLS histograms at the beginning of the experiment and after one week. FL decay curves were fitted using a sum of 3 exponential functions, residuals and χ^2 values are presented.

During the week, PL intensity of cQDs in DMEM decreased by about 40 % and average FL lifetime decreased by about 23 %. Average hydrodynamic diameter decreased from 114 nm to 90 nm (about 21 % decrease).

3.3. Accumulation of quantum dots in live cells

Scanning confocal microscopy images of aQDs accumulated in live MDA-MB-231 breast cancer cells are shown in Fig. 3.8., while images of cQDs accumulated in live U87 glioblastoma cells are shown in Fig. 3.9.

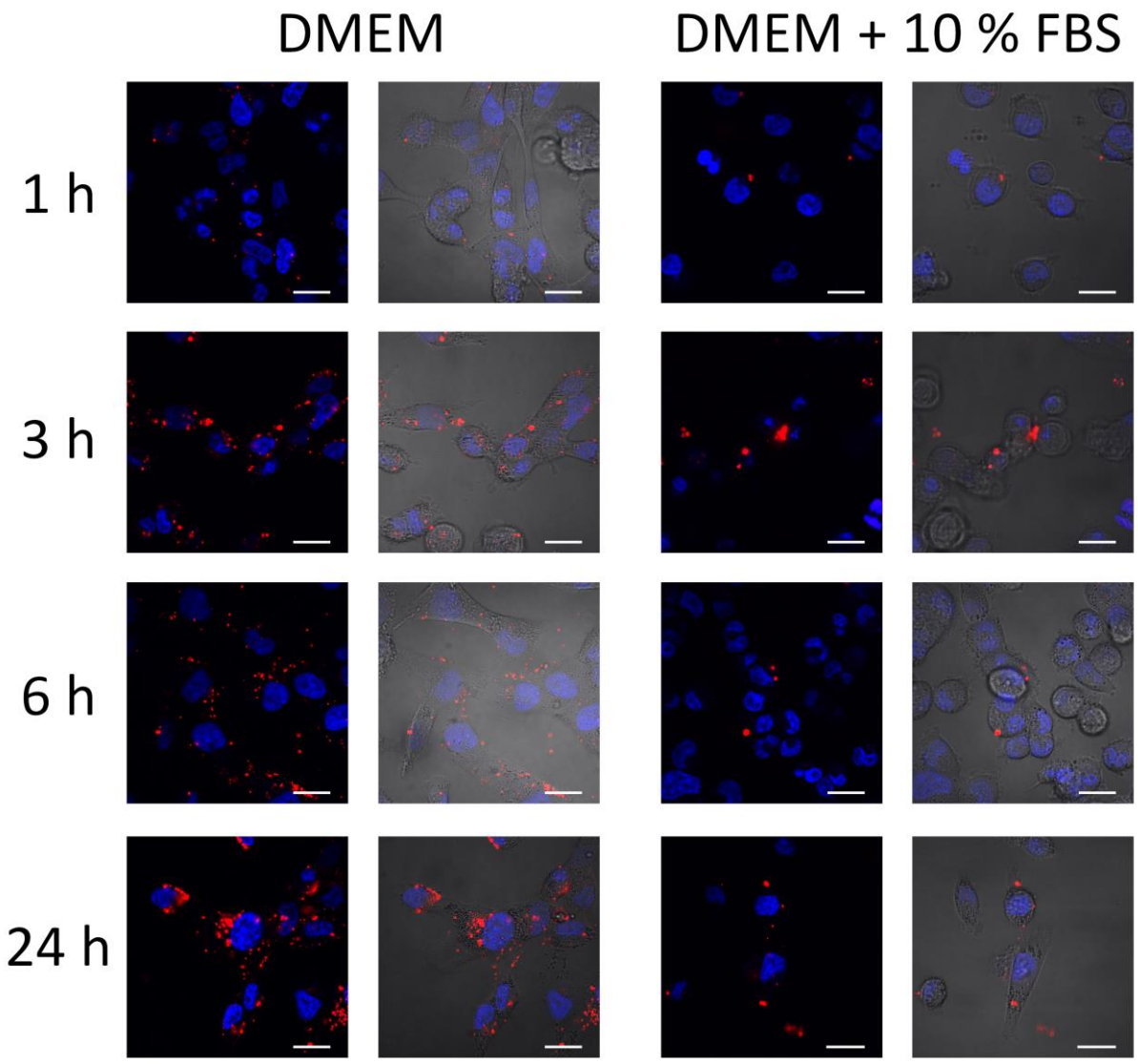

Figure. 3.8. Scanning confocal microscopy images of aQDs accumulated in MDA-MB-231 live cells during different time intervals in serum-free and complete media (both fluorescence and light microscopy images are shown). Blue – cell nuclei, red – QDs. Scale bar – 20 μm.

Accumulation of aQDs in MDA-MB-231 cells shows time dependent behavior and is more efficient in serum-free media. QDs are localized in vesicular structures near cell nuclei.

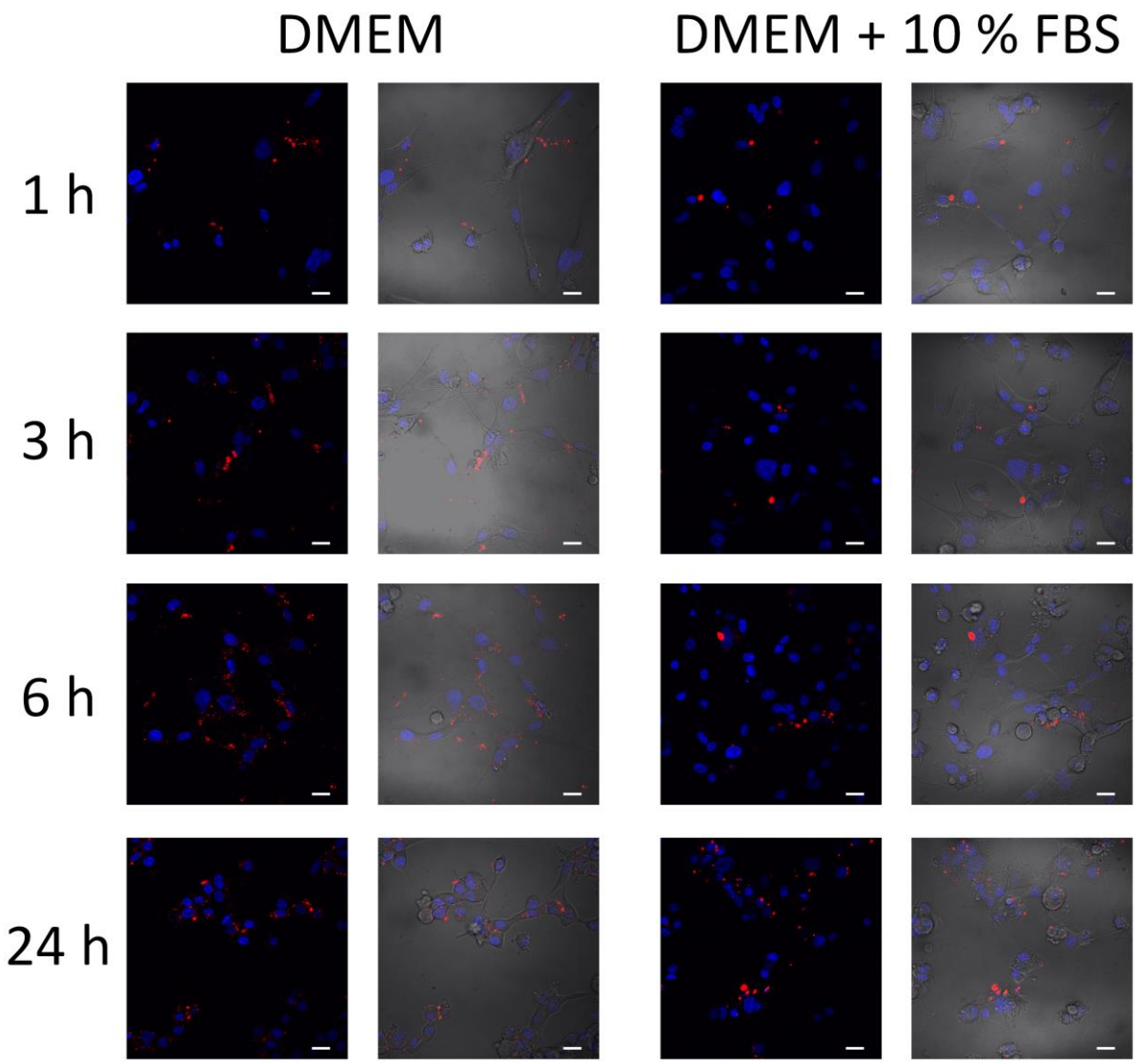

Figure. 3.9. Scanning confocal microscopy images of cQDs accumulated in U87 live cells during different time intervals in serum-free and complete media (both fluorescence and light microscopy images are shown). Blue – cell nuclei, red – QDs. Scale bar – 20 μm.

During the first 6 hours accumulation of cQDs in U87 cells is more efficient in serum-free media than in complete media, while after 24 hours accumulation in both media is similar. Also, accumulation is time dependent in serum-free media. QDs are localized in vesicular structures near cell nuclei.

3.4. Effect of quantum dots on cell viability

Effect of cQDs on U87 cell viability was determined by using XTT viability assay to measure cell proliferation. Results with cells incubated in serum-free and complete media are shown in Figs. 3.10. and 3.11., respectively.

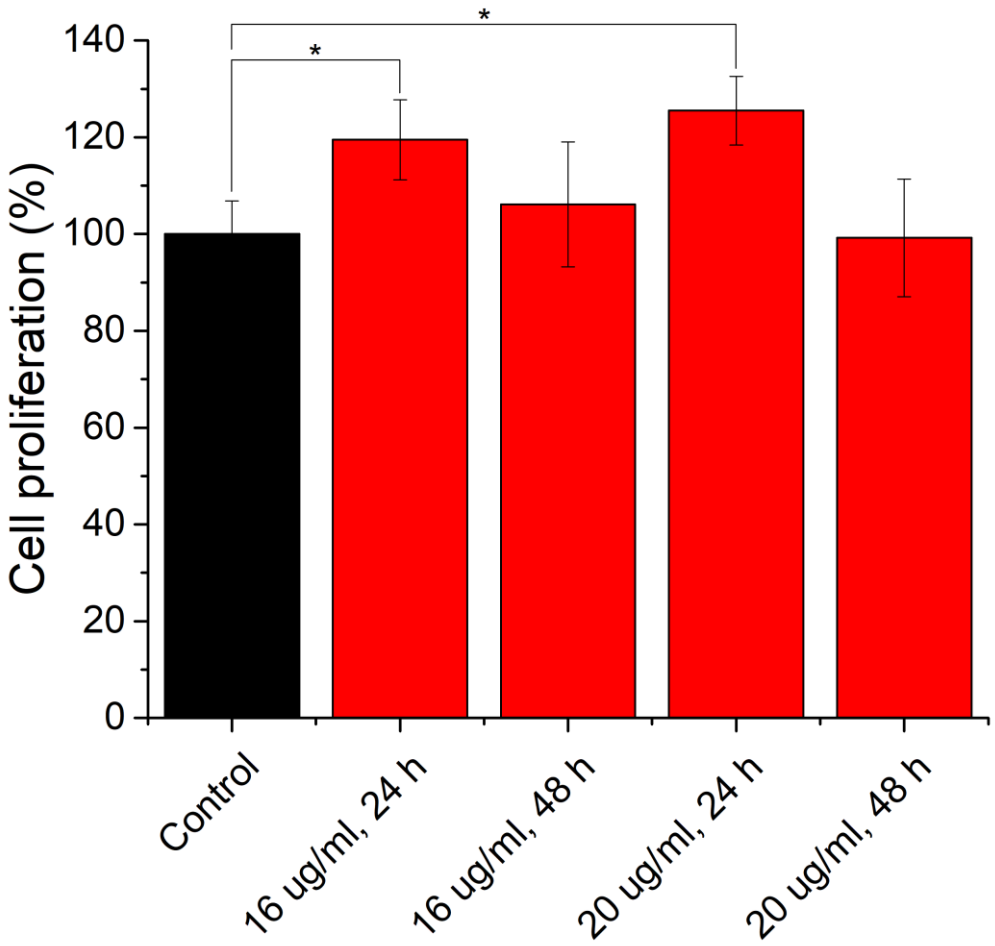

Figure 3.10. Proliferation of U87 cells incubated with different concentrations of cQDs for different time periods in complete media (control – cells incubated without QDs, error bars – standard deviation). Statistically significant differences ($p < 0,05$) are marked.

Compared with control, cell proliferation increased for all tested conditions, except for incubation with 20 μg/ml of QDs for 48 h, were it remained nearly the same as control. After incubation with 16 μg/ml of QDs, proliferation increased to 120 % and 106 % after 24 h and 48 h, respectively. Cell proliferation was the highest after 24 h incubation with 20 μg/ml concentration, reaching 126 %. Cell proliferation after 24 h with both concentrations of QDs was statistically higher compared with control.

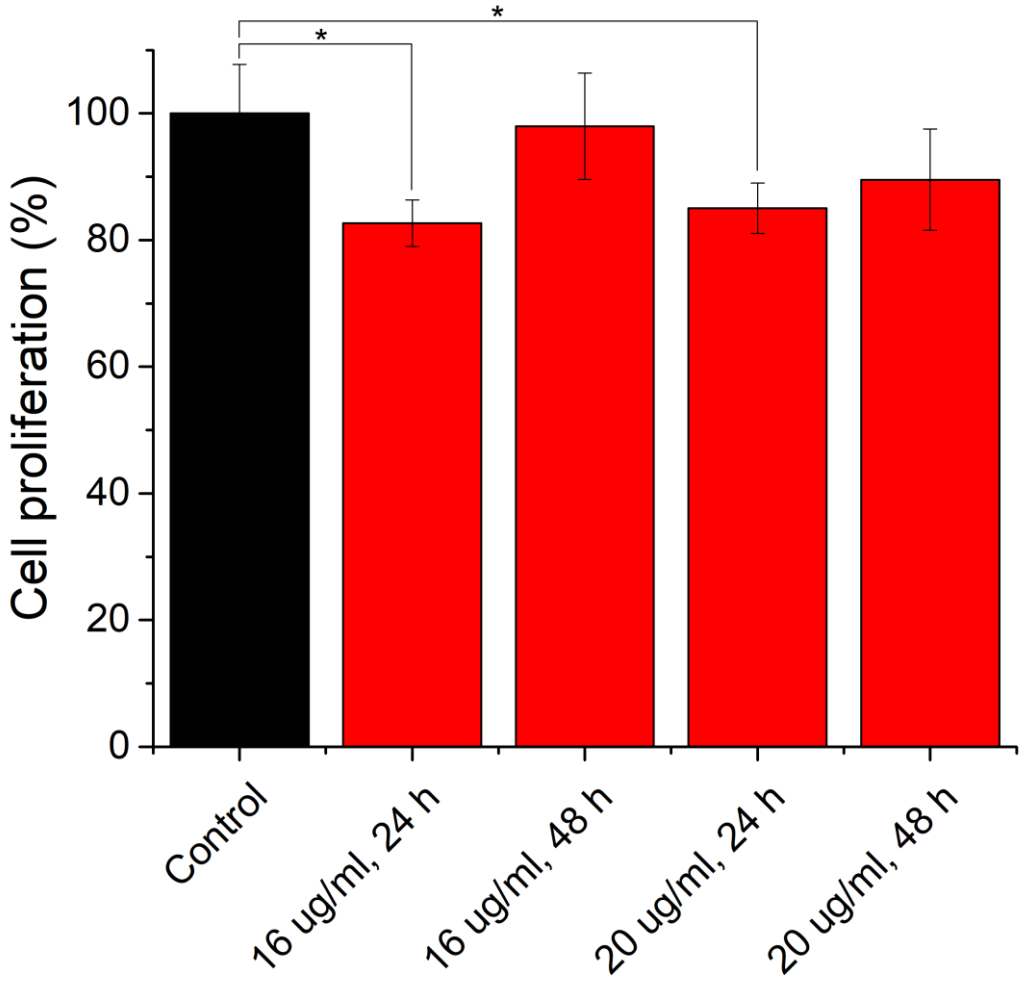

Figure 3.11. Proliferation of U87 cells incubated with different concentrations of cQDs for different time periods in serum-free media (control – cells incubated without QDs, error bars – standard deviation). Statistically significant differences ($p < 0,05$) are marked.

Compared with control, cell proliferation decreased for all tested conditions. With both concentrations of cQDs, cell proliferation decreased to about 85 % after incubation for 24 h. After 48 h incubation, proliferation was 97 % with 16 µg/ml concentration and 90 % with 20 µg/ml concentrations of QDs. Cell proliferation after 24 h with both concentrations of QDs was statistically lower compared with control.

4. DISCUSSION

4.1. Absorption and PL spectra of CIS QDs

Absorption and PL spectra of investigated QDs (Figs. 3.1. and 3.2.) show defining features of CIS QDs - wide absorption ranging from UV to NIR, weak or nonexistent excitonic bands, PL in NIR region and wide PL bands. There are some differences between spectra, though. The absorption spectrum of cQDs is blue shifted compared to aQDs. Possible explanations are different Cu:In ratio or different content of Zn, because these QDs were synthesized in different batches, so their elemental composition may differ. It is known that smaller Cu:In ratio and higher Zn content leads to blue shift of the absorption spectrum of CIS QDs. These factors also affect PL intensity, although the relationship is more complex than in the case of absorption – PL is most intense at an optimal ratio or Zn content value, and deviations decrease PL intensity (Zhang et al., 2015). Because atomic composition of investigated QDs is unknown, it is unclear whether these are the reasons for these differences. Positions of PL peaks also differ, aQDs' peak being centered at 702 nm and cQDs' at 718 nm. This result is surprising, as AFM images show aQDs being more than twice larger than cQDs (Fig. 3.3.), even when disregarding larger particles (assumed to be aggregates of multiple QDs). As these QDs were synthesized on different occasions, their synthesis parameters may differ, and this may account for this discrepancy (Deng et al., 2012). Hydrodynamic diameters of QDs are also much bigger than their sizes measured with AFM – 9 times larger for aQDs and 27 timed for cQDs (Fig. 3.3.). This is in contrast with findings of other groups, which report smaller hydrodynamic diameters (Xia et al., 2017). This could happen if multiple QDs were coated with a single phospholipid layer – larger particles can be seen in AFM images, although this does not explain the missing smaller sized fraction in DLS results.

Comparing both types of QDs, their optical properties are quite similar – absorption spectra are similar, and their PL intensities are of the same order of magnitude (even though the intensity of cQDs is twice that of aQDs). PL peaks of both QDs are in the NIR region, too. These properties are suitable for biomedical applications – wide absorption might allow for multiplex imaging, and PL in NIR is suitable for deep tissue imaging.

4.2. Stability of QDs in PBS and DMEM media

Biological environments contain various compounds, which may have an effect on QDs, such as inducing their aggregation or altering their optical properties. This is an important factor considering their medical applications, as well as *in vitro* experiments using cell cultures, so it has to be investigated. For this reason, we studied stability of QDs in two types of media – PBS and DMEM. PL intensity, FL and hydrodynamic diameter of QDs were measured over a one- week period to observe any changes in these parameters over time. The results are shown in Figs. 3.4 to 3.7. With all QDs, PL intensity and average FL decreased during the week. The largest changes were seen in aQDs in DMEM, where both PL intensity and average FL decreased by about 95 % (Fig. 3.5.). The decrease in PL intensity was not as significant in other cases – from about a quarter for aQDs in PBS (Fig. 3.4.) to about half for cQDs in PBS (Fig. 3.6.). Decreases in average FL were larger in DMEM compared to PBS, where both types of QDs experienced decreases lesser than 10 % (Figs. 3.4. and 3.6.). It can be noticed that average lifetime values were smaller in DMEM than in PBS; this is because of fluorescence of DMEM, as its FL is much shorter than that of QDs (average FL 4 ns). In contrast to this tendency with FL, DLS measurement results show no clear trend, as hydrodynamic diameters increased for aQDs in PBS (Fig. 3.4.) and cQDs in DMEM (Fig. 3.7.), while they decreased for cQDs in PBS (Fig. 3.6.) (it was not possible to properly measure the hydrodynamic diameter of aQDs in DMEM after the week had passed).

A possible explanation of these results is given by Kulvietis et al., who investigated stability of CdTe QDs coated with mercaptopropionic acid. The QDs were mostly stable in deionized water, but in saline or DMEM their PL intensity rapidly decreased. A red shift of PL peak was also observed. Authors propose a hypothesis that these changes are due to QD interaction with cations, which bind to negatively charged mercaptopropionic acid molecules and disrupt the coating, which leads to aggregation and precipitation of QDs (Kulvietis et al., 2011). This might seem to explain the cQD results, because, as CdTe QDs in the cited experiment, their coating contains carboxyl functional groups. However, there are some discrepancies between the results. Even though PL intensity decreased, it did so more slowly than in the experiment by Kulvietis et al. – in their case, it took two days for PL of QDs to completely disappear in saline and one day in DMEM, while in our experiment even after a week PL of cQDs was observed in both media. Red shift, observed in cQDs, was less significant compared to that observed by Kulvietis et al (6 nm is PBS and 8 nm in DMEM in our experiment versus 17 nm in saline and 25 nm in DMEM in Kulvietis' one).

Hydrodynamic diameter of cQDs in DMEM increased, what could be said to indicate their aggregation, but in PBS it decreased instead. No precipitation of QDs was observed, and vortexing had no effect on measured spectra. Also, even though zeta potential of cQDs was much more negative than that of aQDs (about -40 mV vs -5 mV), the stability of QDs did not differ much (in PBS, aQDs were even more stable than cQDs), corroborating that the loss of stability probably was not aggregation of QDs. Composition of saline differs from that of PBS, but their ionic concentrations are very similar, so this difference from Kulvietis' results probably stems from a difference in the QD coating. There is some evidence that phospholipids produce a more stable coating than mercaptopropionic acid (Murcia et al., 2008). This was shown only by an increase in hydrodynamic diameter, though – there were no changes in PL intensity, in contrast to our results. Decrease in FL is also curious, as other authors report no significant changes in FL of CdSe/ZnS QDs following three weeks in PBS, although they used different QD coatings (Lyons et al., 2017).

In the case of aQDs, the results are somewhat more difficult to interpret. While PL intensity and FL decreased as they did with cQDs (only in DMEM they experienced the largest decrease of 95 % after a week), only a slight red shift of a few nm was observed in PBS, while in DMEM the spectrum experienced a small blue shift instead. This is in contrast to DLS results and zeta potential measurements, as hydrodynamic diameter of aQDs in PBS increased to a similar extent as that of cQDs (measurement in DMEM after a week was not possible) and small zeta potential value of aQDs (about -5 mV) shows that QDs tend to aggregate.

Even though stability investigations were carried on for a week, medical applications do not require that much time. In that case, it is reasonable to look at the changes occurring in shorter periods of time (Supplement 1). Changes are not consistent across different QDs and media, but overall, all QDs experienced some decrease in PL intensity, and some had their FL decrease of hydrodynamic diameter change. Despite these changes, both investigated types of QDs should still retain their functionality in this time period, so they should be suitable for medical applications.

4.3. Accumulation of QDs in live cells

As cellular uptake of QDs depends on numerous factors (cell type, QD surface modifications, type of medium), it is necessary to investigate it to ascertain the suitability of QDs for medical applications. To this end, we investigated accumulation of aQDs in MDA-

MB-231 breast cancer cell line and accumulation of cQDs in U87 glioma cell line (it was not possible to study accumulation of aQDs in U87 cells due to quarantine, so an earlier experiment was included). Confocal microscopy images showing accumulation of QDs in cells are presented in Figs. 3.8. and 3.9. for aQDs and cQDs, respectively. Although it is difficult to compare these results due to different QD types and cell lines, some common points can be found. First, the accumulation is time-dependent for both QD types, at least in serum-free media, although it can be seen in complete media, too (clear increase of cQD intracellular concentration seen in Fig. 3.9.). Progress of accumulation resembles that described by Damalakienė et al. – at shorter incubation times, QDs can be seen localized near the plasma membrane, while later they can be observed in vesicular structures near cell nuclei, which shows that endocytosis was the method of uptake (Damalakiene et al., 2013). Another similarity is the differences between accumulation in complete and serum-free media. In both cases, QD uptake was more efficient in serum-free conditions. This difference is not surprising, as it is well known that the protein corona forming on NPs in protein-rich environments influences their interactions with cells (Prapainop et al., 2012). Some authors report similar results – serum interfering with QD uptake in cells and this (Jian et al., 2013), while others found that this had no effect on QD accumulation (Damalakiene et al., 2013). Although formation of protein corona can be seen as a hindrance, it can also be used to enhance NP targeting or increase duration of NP circulation (Peng and Mu, 2016).

4.4. Effect of cQDs on U87 cell viability

Although for quite some time the general consensus was that CIS QDs are less toxic than QDs containing heavy metals, some recent research showing the opposite result cast doubt to this claim, even if only non-shelled QDs were found to be acutely toxic (Kays et al., 2020). These results show that safety of CIS QDs should not be taken for granted, and, to this end, we investigated the effect of cQDs on U87 cell viability both in serum-free and complete media by measuring cell proliferation with XTT assay after incubation with QDs. In complete media (Fig. 3.10.) cell proliferation saw a statistically significant increase after 24 h incubation with QDs but did not differ from control after 48 h incubation. Some authors have also found that CIS QDs can stimulate cell growth, although this effect was observed only at higher QD concentrations (100 μg/ml). Furthermore, they found no difference in viability between cells incubated with QDs for 24 h and 48 h (Chen et al., 2020). This is in stark contrast to our results, where proliferation after 48 h incubation was clearly lower than after

24 h, even though differences were not statistically significant. As authors of this paper used a different cell line (no investigations of CIS QD effect on U87 cell viability were found), it may be a possible reason for these differences. This one paper notwithstanding, most of the other authors find that CIS QDs decrease cell viability (Mir et al., 2018) or have no effect on it (Chen et al., 2015). In our case, similar results were obtained in serum-free media (Fig. 3.11.), where a decrease in cell proliferation was observed in all cases, although only two of them (after 24 h incubation with both concentrations) significantly differed from control. It has to be noted that only investigations in complete media were found, and it is not clear how they compare to our results in serum-free media. Both in complete and serum-free media, we found no difference between different QD concentrations, possibly due to them being quite similar (16 μg/ml and 20 μg/ml).

There are several possible ways to explain the observed difference between cell viabilities in serum-free and complete media. Our experiments on cQD accumulation in U87 cells (Fig. 3.9.) showed more efficient accumulation in serum-free environment, even though after 24 h there was no observable difference between accumulation in serum-free and complete media. If we assume that concentration of QDs in cells incubated in serum-free media was higher, that might be the cause of their lower viability compared with cells incubated in complete media. Another possibility is that QDs can interact with serum constituents and affect cell viability in this way, although this is merely a speculation on the author's part.

4.5. Summary

The aim of this work was to evaluate the potential use of functionalized CIS/ZnS QDs for application in brain cancer theranostics. For the most part, the requirements for that do not differ much from those of theranostics in general: preferably, QDs should photoluminesce in NIR spectral region, have a wide absorption spectrum, be stable in biological environments and be non-toxic. Both types of investigated QDs have optical properties which should be suitable for either imaging or therapeutic applications. Their stability also seems sufficient, as after 1 day both their PL intensity and FL were still adequate for these applications. Accumulation in cells, on the other hand, could use some improvement, as QD uptake in complete media was lower compared to serum-free media. For both aQDs and cQDs in complete media, only after 24 hours QDs were accumulated in both MDA-MB-231 and U87 cells, respectively. As biological environments also contain various proteins, similar results

can be expected *in vivo* as well. On the positive side, formation of protein corona could also be exploited to improve targeting of QDs, although it would require extensive further research (Peng and Mu, 2016). The biggest concern is nanotoxicity of investigated QDs. Although our investigation did not show them to be excessively toxic, results differ quite a bit between serum-free and complete media. Adding the recent research showing that non-shelled CIS QDs are of comparable toxicity to Cd QDs (Kays et al., 2020), it is clear that more experiments are required to fully gauge the safety of these nanomaterials.

4.6. Future perspectives

Even though the results acquired during this work show the potential these QDs possess, further experiments should be performed to see the complete picture. In the literature review, it was mentioned that BBB is a major obstacle in brain cancer theranostics. It is well known that various NPs, including QDs, have some capacity of passing it (Zhou et al., 2018). Seeing as no relevant research regarding CIS QDs was found, we planned to test this capability of theirs by using a simple *in vitro* BBB model comprised of HUVEC endothelial cells (human umbilical vein endothelial cells) grown on a membrane (Fig. 4.1.). Similar BBB models have been extensively used for such purposes (Helms et al., 2016). The plan was to investigate migration of QDs through this artificial BBB and their accumulation in U87 cells. The other planned experiment had to do with the therapeutic side of QD application – we wanted to investigate its use for PDT of U87 cells. The experiment would had involved formation of CIS QD-Ce6 (photosensitizer chlorin e6) complex and evaluation of its stability and effectiveness at destroying U87 cells. We investigated formation of QD-Ce6 complexes in an earlier pilot study using CdSe QDs (Supplement 2). Although these experiments could not be performed for this work due to quarantine restrictions, they may still serve as an excellent guideline for continuation of this experiment.

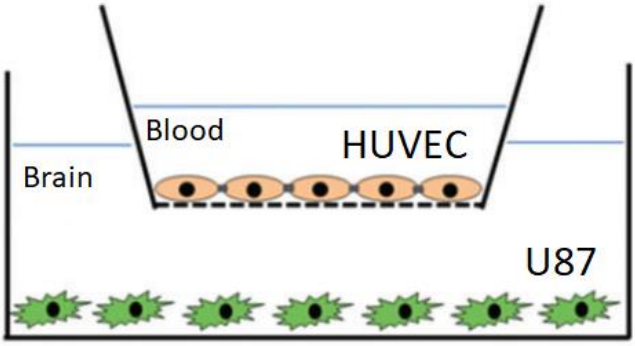

Figure 4.1. Scheme of the BBB model (adapted from (Helms et al., 2016)).

CONCLUSIONS

1. Measured optical (wide absorption band, photoluminescence in near-infrared region, large Stokes shift) and morphological properties of both aminated quantum dots and carboxylated quantum dots are suitable for brain cancer diagnostic applications.

2. Over a one-week investigation of changes in photoluminescence intensity and fluorescence lifetime, aminated quantum dots were found to be more stable in PBS than in DMEM, while carboxylated quantum dots were more stable in DMEM; after 24 h, photoluminescence intensity and fluorescence lifetime of both types of quantum dots were still suitable for application in brain cancer diagnostics.

3. Accumulation of both aminated quantum dots in MDA-MB-231 breast cancer cells and carboxylated quantum dots in U87 glioblastoma cells was more efficient in serum-free media, indicating that interaction between quantum dots and serum proteins can influence quantum dot uptake by cells; also, carboxylated quantum dots were not found to have an overtly negative effect on U87 cell viability.

REFERENCES

1. Abrahamse, H., and Hamblin, M.R. (2016). New photosensitizers for photodynamic therapy. Biochemical Journal *473*, 347–364.

2. Akimoto, J. (2016). Photodynamic Therapy for Malignant Brain Tumors. Neurologia Medico-Chirurgica *56*, 151–157.

3. Allison, R.R., and Moghissi, K. (2013). Photodynamic Therapy (PDT): PDT Mechanisms. Clinical Endoscopy *46*, 24.

4. Brain Tumor: Diagnosis (2019). American Society of Clinical Oncology. Web site, viewed 2020-06-09. Link: https://www.cancer.net/cancer-types/brain-tumor/diagnosis

5. Auner, G.W., Koya, S.K., Huang, C., Broadbent, B., Trexler, M., Auner, Z., Elias, A., Mehne, K.C., and Brusatori, M.A. (2018). Applications of Raman spectroscopy in cancer diagnosis. Cancer Metastasis Rev *37*, 691–717.

6. Bao, X., Yuan, Y., Chen, J., Zhang, B., Li, D., Zhou, D., Jing, P., Xu, G., Wang, Y., Holá, K., et al. (2018). In vivo theranostics with near-infrared-emitting carbon dots—highly efficient photothermal therapy based on passive targeting after intravenous administration. Light Sci Appl *7*, 91.

7. Bera, D., Qian, L., Tseng, T.-K., and Holloway, P.H. (2010). Quantum Dots and Their Multimodal Applications: A Review. Materials *3*, 2260–2345.

8. Blackman, B., Battaglia, D., and Peng, X. (2008). Bright and Water-Soluble Near IR-Emitting CdSe/CdTe/ZnSe Type-II/Type-I Nanocrystals, Tuning the Efficiency and Stability by Growth. Chemistry of Materials *20*, 4847–4853.

9. Bray, F., Ferlay, J., Soerjomataram, I., Siegel, R.L., Torre, L.A., and Jemal, A. (2018). Global cancer statistics 2018: GLOBOCAN estimates of incidence and mortality worldwide for 36 cancers in 185 countries. CA: A Cancer Journal for Clinicians *68*, 394–424.

10. Calixto, G., Bernegossi, J., de Freitas, L., Fontana, C., and Chorilli, M. (2016). Nanotechnology-Based Drug Delivery Systems for Photodynamic Therapy of Cancer: A Review. Molecules *21*, 342.

11. Castano, A.P., Demidova, T.N., and Hamblin, M.R. (2005). Mechanisms in photodynamic therapy: Part three-Photosensitizer pharmacokinetics, biodistribution, tumor localization and modes of tumor destruction. Photodiagnosis Photodyn Ther *2*, 91–106.

12. Chen, C.-W., Wu, D.-Y., Chan, Y.-C., Lin, C.C., Chung, P.-H., Hsiao, M., and Liu, R.-S. (2015). Evaluations of the Chemical Stability and Cytotoxicity of $CuInS_2$ and $CuInS_2$/ZnS Core/Shell Quantum Dots. J. Phys. Chem. C *119*, 2852–2860.

13. Chen, T., Li, L., Lin, X., Yang, Z., Zou, W., Chen, Y., Xu, J., Liu, D., Wang, X., and Lin, G. (2020). *In vitro* and *in vivo* immunotoxicity of PEGylated Cd-free $CuInS_2$/ZnS quantum dots. Nanotoxicology *14*, 372–387.

14. Cheng, Y., Dai, Q., Morshed, R.A., Fan, X., Wegscheid, M.L., Wainwright, D.A., Han, Y., Zhang, L., Auffinger, B., Tobias, A.L., et al. (2014). Blood-Brain Barrier Permeable Gold Nanoparticles: An Efficient Delivery Platform for Enhanced Malignant Glioma Therapy and Imaging. Small n/a-n/a.

15. Damalakiene, L., Karabanovas, Valius, Rotomskis, R., and Bagdonas (2013). Intracellular distribution of nontargeted quantum dots after natural uptake and microinjection. International Journal of Nanomedicine 555.

16. DeAngelis, L.M. (2001). Brain Tumors. New England Journal of Medicine *344*, 114–123.

17. Deng, D., Chen, Y., Cao, J., Tian, J., Qian, Z., Achilefu, S., and Gu, Y. (2012). High-Quality CuInS $_2$ /ZnS Quantum Dots for In vitro and In vivo Bioimaging. Chem. Mater. *24*, 3029–3037.

18. Diaz, R.J., Dios, R.R., Hattab, E.M., Burrell, K., Rakopoulos, P., Sabha, N., Hawkins, C., Zadeh, G., Rutka, J.T., and Cohen-Gadol, A.A. (2015). Study of the biodistribution of fluorescein in glioma-infiltrated mouse brain and histopathological correlation of intraoperative findings in high-grade gliomas resected under fluorescein fluorescence guidance. Journal of Neurosurgery *122*, 1360–1369.

19. Doughty, A., Hoover, A., Layton, E., Murray, C., Howard, E., and Chen, W. (2019). Nanomaterial Applications in Photothermal Therapy for Cancer. Materials *12*, 779.

20. Duchnowska, R., Loibl, S., and Jassem, J. (2018). Tyrosine kinase inhibitors for brain metastases in HER2-positive breast cancer. Cancer Treatment Reviews *67*, 71–77.

21. Ehrhart, F., Evelo, C., and Willighagen, E. (2015). Current systems biology approaches in hazard assessment of nanoparticles. BioRxiv.

22. Fang, M., Peng, C.-W., Pang, D.-W., and Li, Y. (2012). Quantum dots for cancer research: current status, remaining issues, and future perspectives. Cancer Biol Med *9*, 151–163.

23. Feng, Y., Liu, L., Hu, S., Liu, Y., Ren, Y., and Zhang, X. (2016). Förster resonance energy transfer properties of a new type of near-infrared excitation PDT photosensitizer: CuInS $_2$ /ZnS quantum dots-5-aminolevulinic acid conjugates. RSC Advances *6*, 55568–55576.

24. Foda, M.F., Huang, L., Shao, F., and Han, H.-Y. (2014). Biocompatible and Highly Luminescent Near-Infrared CuInS $_2$ /ZnS Quantum Dots Embedded Silica Beads for Cancer Cell Imaging. ACS Applied Materials & Interfaces *6*, 2011–2017.

25. Fox, M. (2006). Quantum optics: an introduction (Oxford ; New York: Oxford University Press), 378 p.

26. Galli, R., Meinhardt, M., Koch, E., Schackert, G., Steiner, G., Kirsch, M., and Uckermann, O. (2019). Rapid Label-Free Analysis of Brain Tumor Biopsies by Near Infrared Raman and Fluorescence Spectroscopy—A Study of 209 Patients. Front. Oncol. *9*, 1165.

27. Garland, M., Yim, J.J., and Bogyo, M. (2016). A Bright Future for Precision Medicine: Advances in Fluorescent Chemical Probe Design and Their Clinical Application. Cell Chemical Biology *23*, 122–136.

28. Haj-Hosseini, N., Richter, J.C.O., Milos, P., Hallbeck, M., and Wårdell, K. (2018). 5-ALA fluorescence and laser Doppler flowmetry for guidance in a stereotactic brain tumor biopsy. Biomed. Opt. Express *9*, 2284.

29. Helms, H.C., Abbott, N.J., Burek, M., Cecchelli, R., Couraud, P.-O., Deli, M.A., Förster, C., Galla, H.J., Romero, I.A., Shusta, E.V., et al. (2016). In vitro models of the blood–brain barrier: An overview of commonly used brain endothelial cell culture models and guidelines for their use. J Cereb Blood Flow Metab *36*, 862–890.

30. Huang, J.H., Zhang, J., and Zager, E.L. (2005). Diagnosis and treatment options for nerve sheath tumors. Expert Review of Neurotherapeutics *5*, 515–523.

31. Jayasundara, S., and Ali, M.M. (2017). Dendrimer-based Nanoparticles for Targeted Brain Tumor Imaging. J Nanomed Nanotechnol *08*.

32. Jermyn, M., Mok, K., Mercier, J., Desroches, J., Pichette, J., Saint-Arnaud, K., Bernstein, L., Guiot, M.-C., Petrecca, K., and Leblond, F. (2015). Intraoperative brain cancer detection with Raman spectroscopy in humans. Science Translational Medicine *7*, 274ra19-274ra19.

33. Jian, Y., Xu, X., Li, Y., and Gu, Z. (2013). Effect of serum on PEGylated quantum dots: Cellular uptake and intracellular distribution. Progress in Natural Science: Materials International *23*, 566–572.

34. Jung, S., Bang, M., Kim, B.S., Lee, S., Kotov, N.A., Kim, B., and Jeon, D. (2014). Intracellular Gold Nanoparticles Increase Neuronal Excitability and Aggravate Seizure Activity in the Mouse Brain. PLoS ONE *9*, e91360.

35. Kantelhardt, S.R., Kalasauskas, D., König, K., Kim, E., Weinigel, M., Uchugonova, A., and Giese, A. (2016). In vivo multiphoton tomography and fluorescence lifetime imaging of human brain tumor tissue. Journal of Neuro-Oncology *127*, 473–482.

36. Kays, J.C., Saeboe, A.M., Toufanian, R., Kurant, D.E., and Dennis, A.M. (2020). Shell-Free Copper Indium Sulfide Quantum Dots Induce Toxicity *in Vitro* and *in Vivo*. Nano Lett. *20*, 1980–1991.

37. Kong, X., Dong, B., Song, X., Wang, C., Zhang, N., and Lin, W. (2018). Dual turn-on fluorescence signal-based controlled release system for real-time monitoring of drug release dynamics in living cells and tumor tissues. Theranostics *8*, 800–811.

38. Kulvietis, V., Streckytė, G., and Rotomskis, R. (2011). Spectroscopic investigations of CdTe quantum dot stability in different aqueous media. Lithuanian Journal of Physics *51*, 163–171.

39. Kut, C., Chaichana, K.L., Xi, J., Raza, S.M., Ye, X., McVeigh, E.R., Rodriguez, F.J., Quiñones-Hinojosa, A., and Li, X. (2015). Detection of human brain cancer infiltration ex vivo and in vivo using quantitative optical coherence tomography. Sci. Transl. Med. *7*, 292ra100-292ra100.

40. Le, V.-H., Yoo, S.W., Yoon, Y., Wang, T., Kim, B., Lee, S., Lee, K.-H., Kim, K.H., and Chung, E. (2017). Brain tumor delineation enhanced by moxifloxacin-based two-photon/CARS combined microscopy. Biomed. Opt. Express *8*, 2148.

41. Li, H., Yu, J., Zhang, R., Hu, W., Li, X., and Zheng, W. (2019). Two-photon excitation fluorescence lifetime imaging microscopy and spectroscopy for cancer detection. In Optics in Health Care and Biomedical Optics IX, Q. Luo, X. Li, Y. Tang, Y. Gu, and D. Zhu, eds. (Hangzhou, China: SPIE), p. 38.

42. Li, J., Liu, C., Hu, Y., Ji, C., Li, S., and Yin, M. (2020). pH-responsive perylenediimide nanoparticles for cancer trimodality imaging and photothermal therapy. Theranostics *10*, 166–178.

43. Li, X., Tsibouklis, J., Weng, T., Zhang, B., Yin, G., Feng, G., Cui, Y., Savina, I.N., Mikhalovska, L.I., Sandeman, S.R., et al. (2017). Nano carriers for drug transport across the blood–brain barrier. Journal of Drug Targeting *25*, 17–28.

44. Liu, Y., Ma, K., Jiao, T., Xing, R., Shen, G., and Yan, X. (2017). Water-Insoluble Photosensitizer Nanocolloids Stabilized by Supramolecular Interfacial Assembly towards Photodynamic Therapy. Scientific Reports *7*.

45. Liu, Y., Liu, J., Zhang, J., Li, X., Lin, F., Zhou, N., Yang, B., and Lu, L. (2018). Noninvasive Brain Tumor Imaging Using Red Emissive Carbonized Polymer Dots across the Blood–Brain Barrier. ACS Omega *3*, 7888–7896.

46. Liu, Z., Ren, G., Zhang, T., and Yang, Z. (2009). Action potential changes associated with the inhibitory effects on voltage-gated sodium current of hippocampal CA1 neurons by silver nanoparticles. Toxicology *264*, 179–184.

47. Liu, Z., Zhang, T., Ren, G., and Yang, Z. (2012). Nano-Ag inhibiting action potential independent glutamatergic synaptic transmission but increasing excitability in rat CA1 pyramidal neurons. Nanotoxicology *6*, 414–423.

48. Louis, D.N., Perry, A., Reifenberger, G., von Deimling, A., Figarella-Branger, D., Cavenee, W.K., Ohgaki, H., Wiestler, O.D., Kleihues, P., and Ellison, D.W. (2016). The 2016 World Health Organization Classification of Tumors of the Central Nervous System: a summary. Acta Neuropathologica *131*, 803–820.

49. Lucky, S.S., Soo, K.C., and Zhang, Y. (2015). Nanoparticles in Photodynamic Therapy. Chemical Reviews *115*, 1990–2042.

50. Lv, G., Guo, W., Zhang, W., Zhang, T., Li, S., Chen, S., Eltahan, A.S., Wang, D., Wang, Y., Zhang, J., et al. (2016). Near-Infrared Emission CuInS/ZnS Quantum Dots: All-in-One Theranostic Nanomedicines with Intrinsic Fluorescence/Photoacoustic Imaging for Tumor Phototherapy. ACS Nano *10*, 9637–9645.

51. Lyons, T.Y., Williams, D.N., and Rosenzweig, Z. (2017). Addition of Fluorescence Lifetime Spectroscopy to the Tool Kit Used to Study the Formation and Degradation of Luminescent Quantum Dots in Solution. Langmuir *33*, 3018–3027.

52. Maiti, D., Tong, X., Mou, X., and Yang, K. (2019). Carbon-Based Nanomaterials for Biomedical Applications: A Recent Study. Front. Pharmacol. *9*, 1401.

53. Quantum Dots for Electronics and Energy Applications | Sigma Aldrich. Marat Lutfullin, and Osman M. Bakr. Web site, viewed 2020-06-09. Link: https://www.sigmaaldrich.com/technical-documents/articles/materials-science/quantum-dots-noncadmium.html

54. McFaline-Figueroa, J.R., and Lee, E.Q. (2018). Brain Tumors. The American Journal of Medicine *131*, 874–882.

55. McHugh, K.J., Jing, L., Behrens, A.M., Jayawardena, S., Tang, W., Gao, M., Langer, R., and Jaklenec, A. (2018). Biocompatible Semiconductor Quantum Dots as Cancer Imaging Agents. Advanced Materials *30*, 1706356.

56. Michalska, M., Florczak, A., Dams-Kozlowska, H., Gapinski, J., Jurga, S., and Schneider, R. (2016). Peptide-functionalized ZCIS QDs as fluorescent nanoprobe for targeted HER2-positive breast cancer cells imaging. Acta Biomaterialia *35*, 293–304.

57. Mir, I.A., Das, K., Akhter, T., Ranjan, R., Patel, R., and Bohidar, H.B. (2018). Eco-friendly synthesis of $CuInS_2$ and $CuInS_2$ @ZnS quantum dots and their effect on enzyme activity of lysozyme. RSC Adv. *8*, 30589–30599.

58. Mo, D., Hu, L., Zeng, G., Chen, G., Wan, J., Yu, Z., Huang, Z., He, K., Zhang, C., and Cheng, M. (2017). Cadmium-containing quantum dots: properties, applications, and toxicity. Applied Microbiology and Biotechnology *101*, 2713–2733.

59. Molitch, M.E. (2017). Diagnosis and Treatment of Pituitary Adenomas: A Review. JAMA *317*, 516.

60. Moskovits, M. (2005). Surface-enhanced Raman spectroscopy: a brief retrospective. J. Raman Spectrosc. *36*, 485–496.

61. Murcia, M.J., Minner, Daniel.E., Mustata, G.-M., Ritchie, K., and Naumann, C.A. (2008). Design of Quantum Dot-Conjugated Lipids for Long-Term, High-Speed Tracking Experiments on Cell Surfaces. J. Am. Chem. Soc. *130*, 15054–15062.

62. Naghavi, M., Abajobir, A.A., Abbafati, C., Abbas, K.M., Abd-Allah, F., Abera, S.F., Aboyans, V., Adetokunboh, O., Afshin, A., Agrawal, A., et al. (2017). Global, regional, and national age-sex specific mortality for 264 causes of death, 1980–2016: a systematic analysis for the Global Burden of Disease Study 2016. The Lancet *390*, 1151–1210.

63. Nurunnabi, M., Khatun, Z., Huh, K.M., Park, S.Y., Lee, D.Y., Cho, K.J., and Lee, Y. (2013). *In Vivo* Biodistribution and Toxicology of Carboxylated Graphene Quantum Dots. ACS Nano *7*, 6858–6867.

64. Patra, J.K., Das, G., Fraceto, L.F., Campos, E.V.R., Rodriguez-Torres, M. del P., Acosta-Torres, L.S., Diaz-Torres, L.A., Grillo, R., Swamy, M.K., Sharma, S., et al. (2018). Nano based drug delivery systems: recent developments and future prospects. J Nanobiotechnol *16*, 71.

65. Patrice, T. (2004). Photodynamic Therapy. (Cambridge; Secaucus: Royal Society of Chemistry, The Springer [distributor), 284 p.

66. Peng, Q., and Mu, H. (2016). The potential of protein–nanomaterial interaction for advanced drug delivery. Journal of Controlled Release *225*, 121–132.

67. Perkins, A., and Liu, G. (2016). Primary Brain Tumors in Adults: Diagnosis and Treatment. Am Fam Physician *93*, 211–217.

68. Perry, S.W., Burke, R.M., and Brown, E.B. (2012). Two-Photon and Second Harmonic Microscopy in Clinical and Translational Cancer Research. Ann Biomed Eng *40*, 277–291.

69. Pons, T., Pic, E., Lequeux, N., Cassette, E., Bezdetnaya, L., Guillemin, F., Marchal, F., and Dubertret, B. (2010). Cadmium-Free CuInS $_2$ /ZnS Quantum Dots for Sentinel Lymph Node Imaging with Reduced Toxicity. ACS Nano *4*, 2531–2538.

70. Poulon, F., Metais, C., Jamme, F., Zanello, M., Varlet, P., Devaux, B., Refregiers, M., and Abi Haidar, D. (2017). Detection of human brain tumor infiltration with multimodal multiscale optical analysis. A. Mahadevan-Jansen, T. Vo-Dinh, and W.S. Grundfest, eds. (San Francisco, California, United States), p. 100540I.

71. Quantum Dots: Theory, Application, Synthesis (2013). Pranjal Vachaspati. Web site, viewed 2020-06-09. Link: https://pranjalv.com/qdots.pdf

72. Prapainop, K., Witter, D.P., and Wentworth, P. (2012). A Chemical Approach for Cell-Specific Targeting of Nanomaterials: Small-Molecule-Initiated Misfolding of Nanoparticle Corona Proteins. J. Am. Chem. Soc. *134*, 4100–4103.

73. Quirk, B.J., Brandal, G., Donlon, S., Vera, J.C., Mang, T.S., Foy, A.B., Lew, S.M., Girotti, A.W., Jogal, S., LaViolette, P.S., et al. (2015). Photodynamic therapy (PDT) for malignant brain tumors – Where do we stand? Photodiagnosis and Photodynamic Therapy *12*, 530–544.

74. Richter, J.C.O., Haj-Hosseini, N., Hallbeck, M., and Wårdell, K. (2017). Combination of hand-held probe and microscopy for fluorescence guided surgery in the brain tumor marginal zone. Photodiagnosis and Photodynamic Therapy *18*, 185–192.

75. Cancer - Our World in Data (2018). Roser, M., and Ritchie, H. Web site, viewed 2020-06-09. Link: https://ourworldindata.org/cancer#

76. Sharma, K. (2017). Nanomaterials for Drug Delivery. In Advances in Personalized Nanotherapeutics, A. Kaushik, R.D. Jayant, and M. Nair, eds. (Cham: Springer International Publishing), pp. 57–77.

77. Sheng, Y., Li, S., Duan, Z., Zhang, R., and Xue, J. (2018). Fluorescent magnetic nanoparticles as minimally-invasive multi-functional theranostic platform for fluorescence imaging, MRI and magnetic hyperthermia. Materials Chemistry and Physics *204*, 388–396.

78. Shi, D., Mi, G., Shen, Y., and Webster, T.J. (2019). Glioma-targeted dual functionalized thermosensitive Ferri-liposomes for drug delivery through an *in vitro* blood–brain barrier. Nanoscale *11*, 15057–15071.

79. Shi, J., Tian, F., Lyu, J., and Yang, M. (2015). Nanoparticle based fluorescence resonance energy transfer (FRET) for biosensing applications. Journal of Materials Chemistry B *3*, 6989–7005.

80. Smith, B.R., and Gambhir, S.S. (2017). Nanomaterials for In Vivo Imaging. Chemical Reviews *117*, 901–986.

81. Solomon, M., Liu, Y., Berezin, M.Y., and Achilefu, S. (2011). Optical Imaging in Cancer Research: Basic Principles, Tumor Detection, and Therapeutic Monitoring. Med Princ Pract *20*, 397–415.

82. Su, S., and Kang, P.M. (2020). Systemic Review of Biodegradable Nanomaterials in Nanomedicine. Nanomaterials *10*, 656.

83. Su, S., Wang, J., Wei, J., Martínez-Zaguilán, R., Qiu, J., and Wang, S. (2015). Efficient photothermal therapy of brain cancer through porphyrin functionalized graphene oxide. New J. Chem. *39*, 5743–5749.

84. Tartakovskiĭ, A.G. (2012). Quantum dots: optics, electron transport, and future applications (Cambridge ; New York: Cambridge University Press), 358 p.

85. True, L.D., and Gao, X. (2007). Quantum Dots for Molecular Pathology. The Journal of Molecular Diagnostics *9*, 7–11.

86. Tsolekile, N., Ncapayi, V., Parani, S., Sakho, E.H.M., Matoetoe, M.C., Songca, S.P., and Oluwafemi, O.S. (2018). Synthesis of fluorescent CuInS2/ZnS quantum dots—porphyrin conjugates for photodynamic therapy. MRS Communications *8*, 398–403.

87. Valanciunaite, J., Skripka, A., Streckyte, G., and Rotomskis, R. (2010). Complex of water-soluble CdSe/ZnS quantum dots and chlorin e 6 : interaction and FRET. M. Kinnunen, and R. Myllylä, eds. (Oulu, Finland), p. 737607.

88. Vasefi, F., MacKinnon, N., Farkas, D.L., and Kateb, B. (2016). Review of the potential of optical technologies for cancer diagnosis in neurosurgery: a step toward intraoperative neurophotonics. Neurophotonics *4*, 011010.

89. van Veggel, F.C.J.M. (2014). Near-Infrared Quantum Dots and Their Delicate Synthesis, Challenging Characterization, and Exciting Potential Applications. Chemistry of Materials *26*, 111–122.

90. Wang, H., Mu, Q., Wang, K., Revia, R.A., Yen, C., Gu, X., Tian, B., Liu, J., and Zhang, M. (2019). Nitrogen and boron dual-doped graphene quantum dots for near-infrared second window imaging and photothermal therapy. Applied Materials Today *14*, 108–117.

91. Wang, J., Xu, Y., and Boppart, S.A. (2017). Review of optical coherence tomography in oncology. J. Biomed. Opt. *22*, 1.

92. Weissleder, R. (2001). A clearer vision for in vivo imaging. Nature Biotechnology *19*, 316–317.

93. Weller, M., Wick, W., Aldape, K., Brada, M., Berger, M., Pfister, S.M., Nishikawa, R., Rosenthal, M., Wen, P.Y., Stupp, R., et al. (2015). Glioma. Nature Reviews Disease Primers *1*.

94. Wu, Q., Chu, M., Shao, Y., Wo, F., and Shi, D. (2016). Reduced graphene oxide conjugated with CuInS 2 /ZnS nanocrystals with low toxicity for enhanced photothermal and photodynamic cancer therapies. Carbon *108*, 21–37.

95. Xia, C., Meeldijk, J.D., Gerritsen, H.C., and de Mello Donega, C. (2017). Highly Luminescent Water-Dispersible NIR-Emitting Wurtzite CuInS $_2$ /ZnS Core/Shell Colloidal Quantum Dots. Chemistry of Materials *29*, 4940–4951.

96. Yaghini, E., Seifalian, A.M., and MacRobert, A.J. (2009). Quantum dots and their potential biomedical applications in photosensitization for photodynamic therapy. Nanomedicine *4*, 353–363.

97. Yang, Y., Jing, L., Li, X., Lin, L., Yue, X., and Dai, Z. (2017). Hyaluronic Acid Conjugated Magnetic Prussian Blue@Quantum Dot Nanoparticles for Cancer Theranostics. Theranostics *7*, 466–481.

98. Yu, W.W., Chang, E., Drezek, R., and Colvin, V.L. (2006). Water-soluble quantum dots for biomedical applications. Biochemical and Biophysical Research Communications *348*, 781–786.

99. Zhang, B., Wang, Y., Yang, C., Hu, S., Gao, Y., Zhang, Y., Wang, Y., Demir, H.V., Liu, L., and Yong, K.-T. (2015). The composition effect on the optical properties of aqueous synthesized Cu–In–S and Zn–Cu–In–S quantum dot nanocrystals. Phys. Chem. Chem. Phys. *17*, 25133–25141.

100. Zhang, J., Hao, G., Yao, C., Hu, S., Hu, C., and Zhang, B. (2016). Paramagnetic albumin decorated CuInS $_2$ /ZnS QDs for CD133 $^+$ glioma bimodal MR/fluorescence targeted imaging. Journal of Materials Chemistry B *4*, 4110–4118.

101. Zhang, M., Wang, W., Cui, Y., Zhou, N., and Shen, J. (2018). Near-infrared light-mediated photodynamic/photothermal therapy nanoplatform by the assembly of Fe_3O_4 carbon dots with graphitic black phosphorus quantum dots. IJN *Volume 13*, 2803–2819.

102. Zhou, Y., Peng, Z., Seven, E.S., and Leblanc, R.M. (2018). Crossing the blood-brain barrier with nanoparticles. Journal of Controlled Release *270*, 290–303.

103. Zhou, Y., Liu, C.-H., Zhu, K., Wu, B., Yu, X., Cheng, G., Zhao, M., Zong, R., Zhang, C., Chen, H., et al. (2019). Human brain glioma grading using label free laser-induced fluorescence spectroscopy. In Optical Biopsy XVII: Toward Real-Time Spectroscopic Imaging and Diagnosis, R.R. Alfano, S.G. Demos, and A.B. Seddon, eds. (San Francisco, United States: SPIE), p. 46.

104. Zottel, A., Videtič Paska, A., and Jovčevska, I. (2019). Nanotechnology Meets Oncology: Nanomaterials in Brain Cancer Research, Diagnosis and Therapy. Materials *12*, 1588.

105. Zou, L., Wang, H., He, B., Zeng, L., Tan, T., Cao, H., He, X., Zhang, Z., Guo, S., and Li, Y. (2016). Current Approaches of Photothermal Therapy in Treating Cancer Metastasis with Nanotherapeutics. Theranostics *6*, 762–772.

ABSTRACT

During the search for new ways to diagnose and treat cancer, including nervous system cancer, optical methods, such as fluorescence spectroscopy or photodynamic therapy, have emerged as viable alternatives to MRI, radiotherapy and other currently used methods. Such methods require the use of certain organic compounds, namely fluorescent dyes and photosensitizers, and their disadvantages, such as lack of stability in biological environments, hydrophobicity and generally low efficiency, are preventing wider application of optical methods. Use of nanomaterials, like quantum dots (QDs), is one way to improve on these aspects, either by using QDs by themselves or by conjugating them with various other compounds. Their one drawback is possible nanotoxicity, as most widely used QDs contain toxic elements, such as cadmium or lead. This could be circumvented by using heavy metal-free QDs, such as ones composed of $CuInS_2$. As the use of these QDs for cancer theranostics in general is not well investigated, it was decided to investigate their potential as brain cancer theranostic agents. Optical and physicochemical properties of $CuInS_2$/ZnS core/shell QDs functionalized with amine or carboxyl groups were determined using absorption and fluorescence spectroscopy, atomic force microscopy and dynamic light scattering methods and were found to be suitable for brain cancer theranostics. Stability of photoluminescence intensity and fluorescence lifetime of both types of QDs over one week was investigated in PBS and DMEM media. aQDs were found to be more stable in PBS, while stability of cQDs was better in DMEM. During the practically important time period of 24 h, stability of both aQDs and cQDs was sufficient for medical applications. Lastly, accumulation of aQDs in MDA-MB-231 breast cancer cells and cQDs in U87 glioblastoma cells was investigated. Results show increasing concentration of QDs inside cells with longer incubation periods, localization of QDs in vesicular structures and more efficient accumulation in serum-free media. cQDs also were shown to not have a negative impact on U87 cell viability. Results of these experiments show the potential of $CuInS_2$ QDs for applications in brain cancer theranostics, although further studies are required to bring them closer to clinical use.

SANTRAUKA

Ieškant naujų metodų įvairių rūšių vėžio, tarp jų ir nervų sistemos vėžio, diagnostikai ir terapijai, optiniai metodai, pavyzdžiui, fluorescencijos spektroskopija ar fotodinaminė terapija, pradėti taikyti kaip alternatyva magnetinio rezonanso tomografijai, radioterapijai ir kitiems šiuo metu naudojamiems metodams. Taikant optinius metodus yra naudojami įvairūs organiniai junginiai (fluorescuojantys dažai ir fotosensibilizatoriai), kurių trūkumai – žemas stabilumas biologinėse terpėse, hidrofobiškumas ir žemas efektyvumas – trukdo platesniam šių metodų pritaikymui. Nanomedžiagos, pavyzdžiui, kvantiniai taškai (KT), yra vienas iš šių trūkumų sprendimo būdų – gali būti naudojami patys KT arba jų ir kitų junginių dariniai. Vienas iš KT trūkumų yra galimas nanotoksiškumas, nes daugumos plačiai naudojamų KT sudėtyje yra toksiškų cheminių elementų, pavyzdžiui, kadmio ar švino. Ši problema gali būti išspręsta naudojant sunkiųjų metalų neturinčius KT, pavyzdžiui, sudarytus iš $CuInS_2$. Tokių KT naudojimas vėžio teranostikai nėra gerai ištirtas, todėl, buvo nuspręsta ištirti jų pritaikymo smegenų vėžio teranostikai potencialą. Amino (aKT) ir karboksilo (cKT) grupėmis funkcionalizuotų $CuInS_2$/ZnS šerdies/apvalkalo KT optinės ir fizikocheminės savybės buvo ištirtos naudojant sugerties ir fluorescencijos spektroskopijos, atominės jėgos mikroskopijos ir dinaminės šviesos sklaidos metodus; savybės buvo tinkamos smegenų vėžio teranostikai. Buvo ištirtas abiejų tipų KT fotoliuminescencijos intensyvumo ir fluorescencijos gyvavimo trukmės stabilumas vienos savaitės laikotarpiu PBS ir DMEM terpėse. aKT buvo stabilesni PBS terpėje, tuo tarpu cKT – DMEM terpėje. Per taikymui svarbų 24 h laiko tarpą abiejų tipų KT stabilumas buvo pakankamas medicininiam taikymui. Galiausiai buvo ištirtas aKT kaupimasis MDA-MB-231 krūties vėžio ląstelėse ir cKT kaupimasis U87 glioblastomos ląstelėse. Rezultatai rodo kartu su inkubacijos laikotarpiu didėjančia KT koncentraciją ląstelėse, KT lokalizaciją pūslelių tipo struktūrose ir efektyvesnį kaupimąsi beseruminėje terpėje. cKT neturėjo neigiamo poveikio U87 ląstelių gyvybingumui. Šių tyrimų rezultatai rodo $CuInS_2$ KT potencialą taikymui smegenų vėžio teranostikoje, bet norint tai pasiekti reikalingi tolimesni tyrimai.

SUPPLEMENTS

Supplement 1: Stability of CIS QDs in PBS and DMEM

FL decay curves and DLS histograms of aQDs and cQDs in PBS or DMEM media after 24 h, 48 h, 72 h and 96 h are shown in Figs. S1.1. to S1.4.

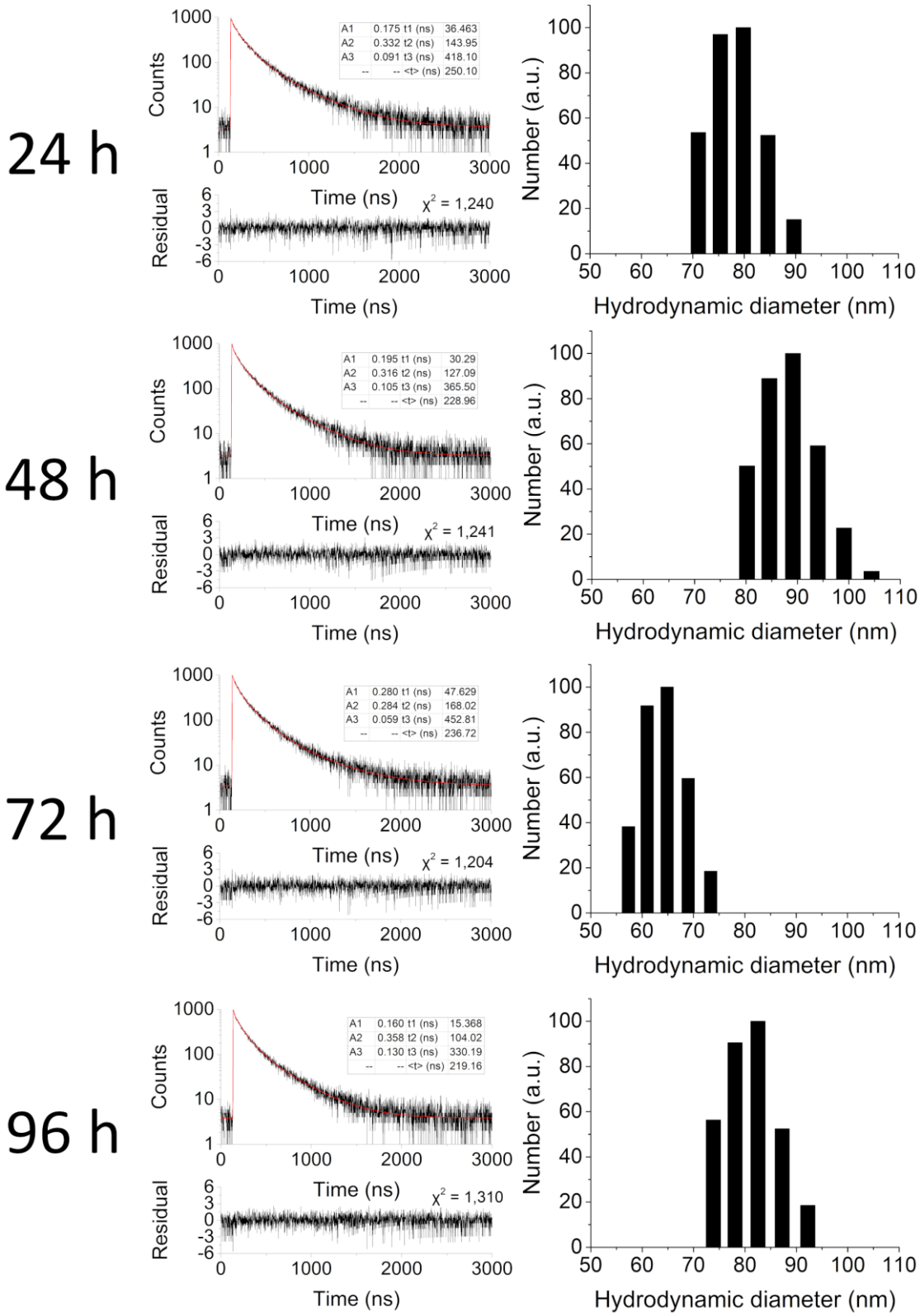

Figure S1.1. FL decay curves and DLS histograms of aQDs in PBS at 24 h, 48 h, 72 h and 96 h. FL decay curves were fitted using a sum of 3 exponential functions, residuals and χ^2 values are presented.

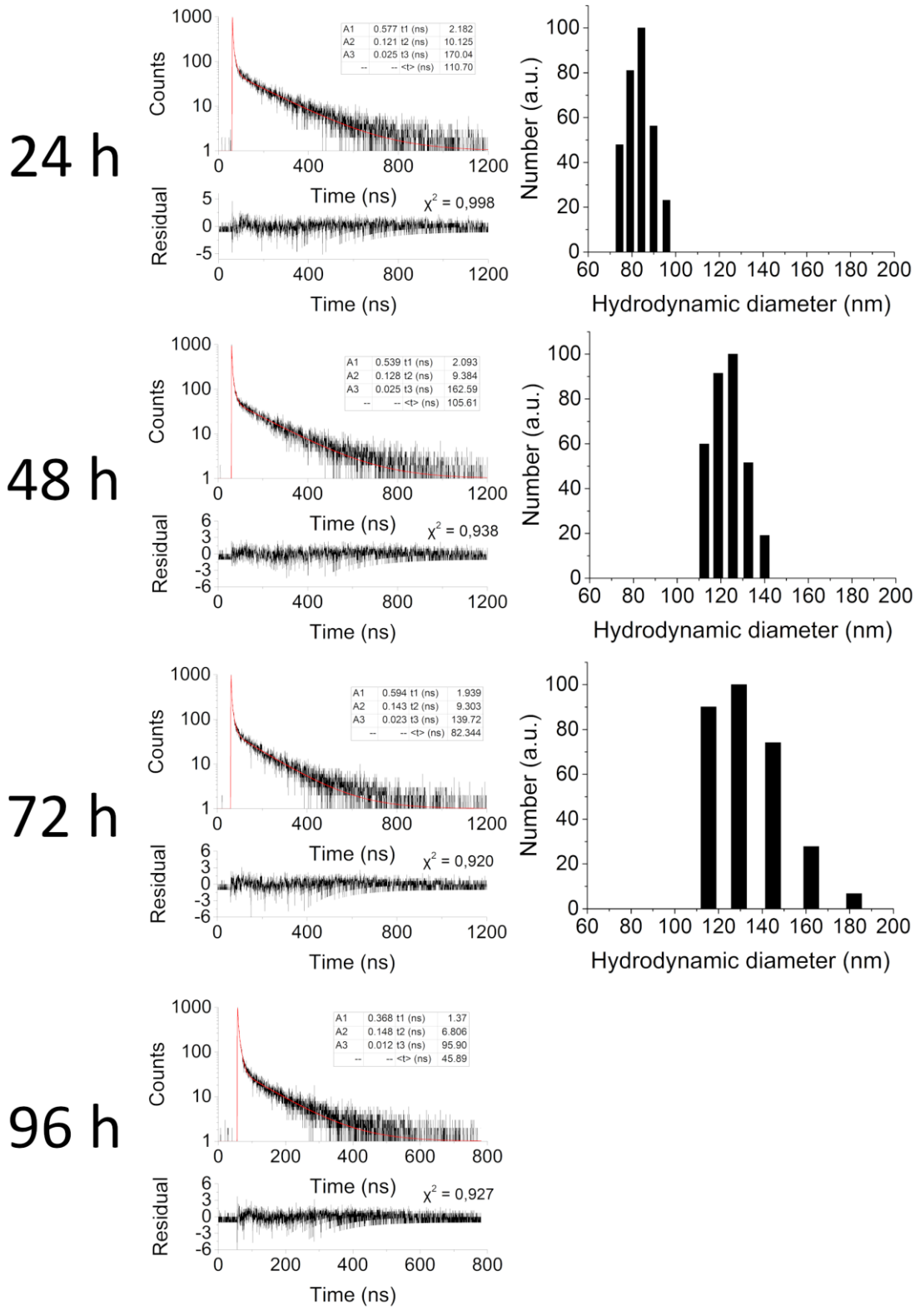

Figure S1.2. FL decay curves and DLS histograms of aQDs in DMEM at 24 h, 48 h, 72 h and 96 h. FL decay curves were fitted using a sum of 3 exponential functions, residuals and χ^2 values are presented. DLS histogram at 96 h could not be properly measured.

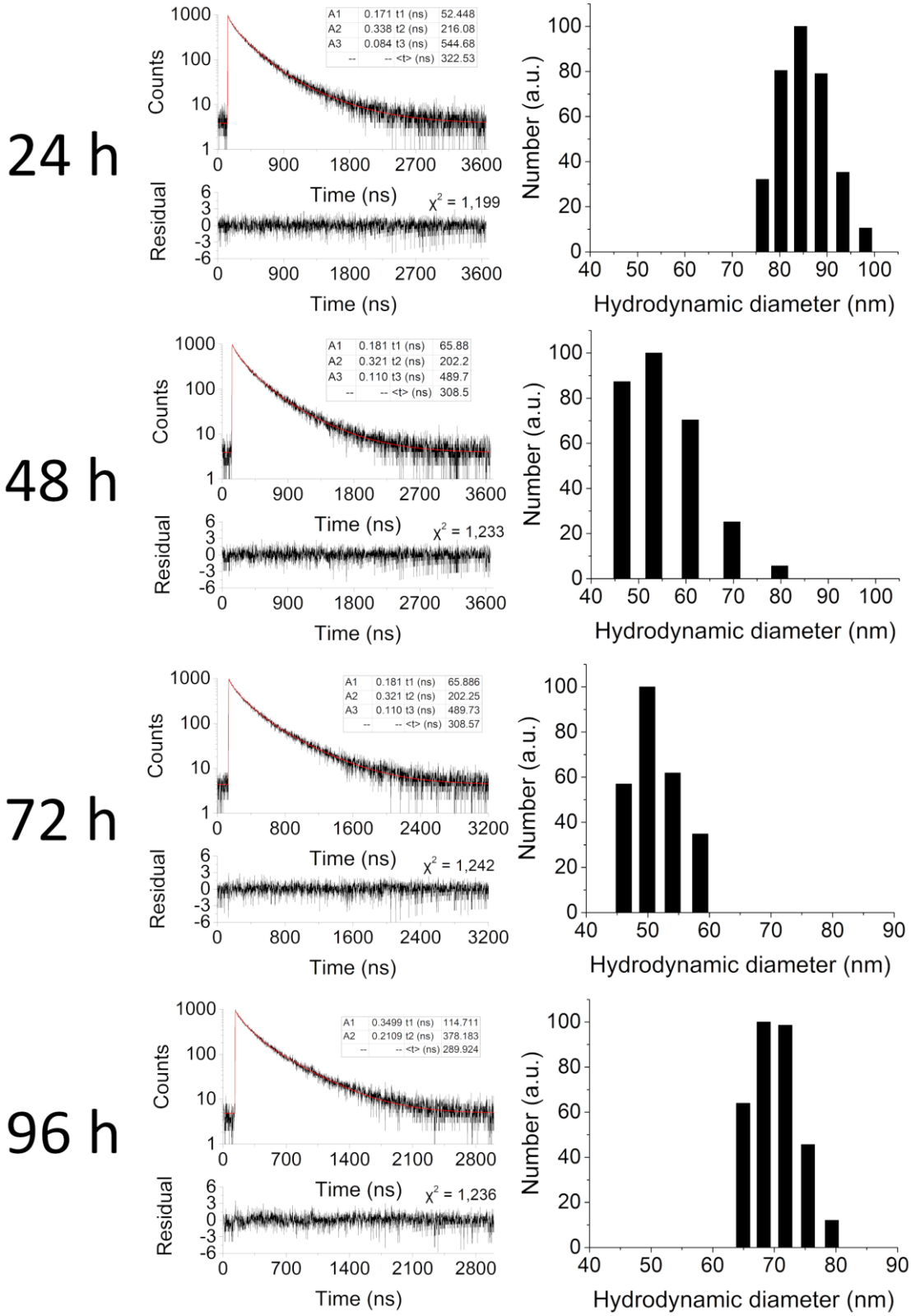

Figure S1.3. FL decay curves and DLS histograms of cQDs in PBS at 24 h, 48 h, 72 h and 96 h. FL decay curves were fitted using a sum of 3 exponential functions (2 for FL decay curve at 96 h), residuals and χ^2 values are presented.

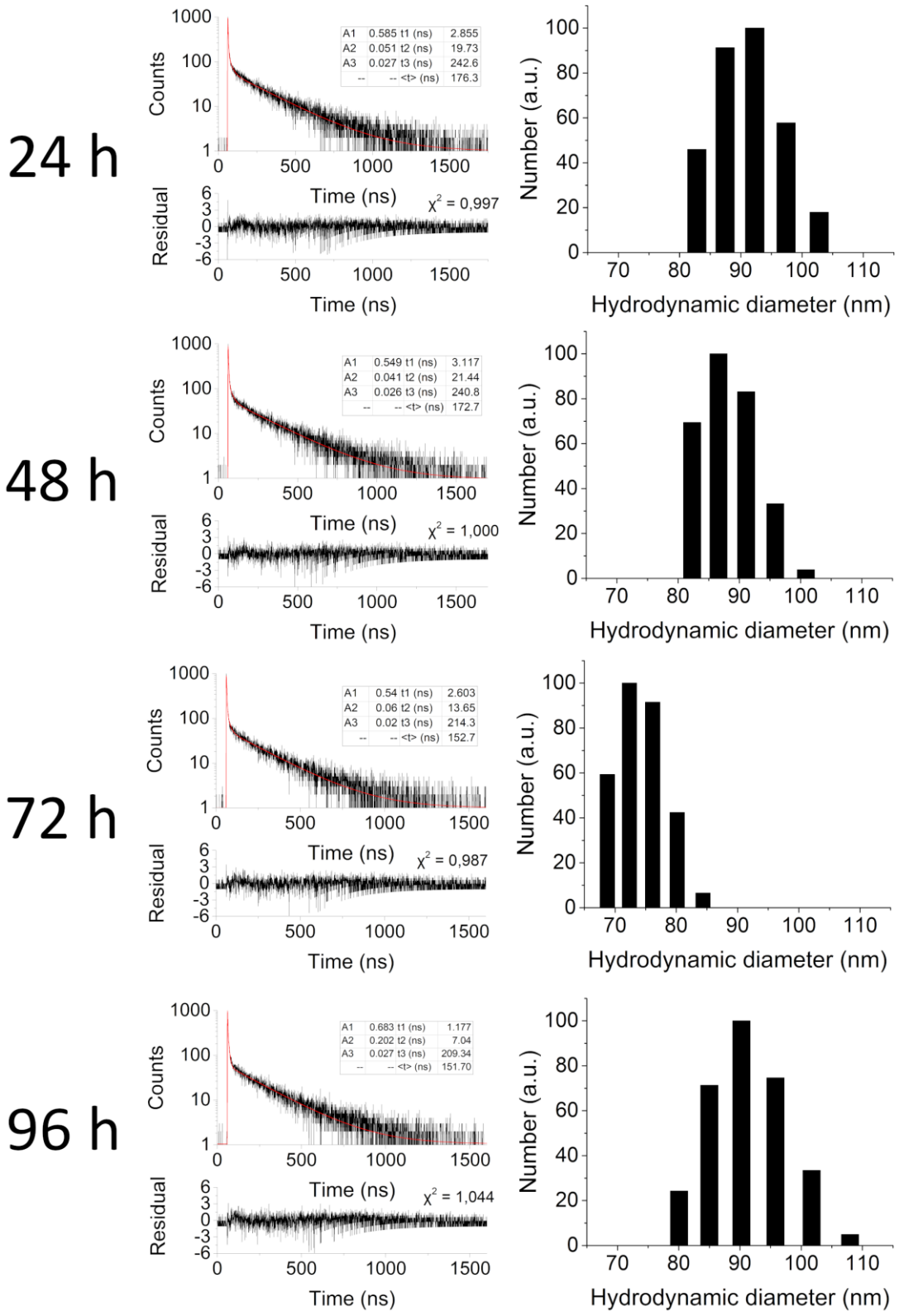

Figure S1.4. FL decay curves and DLS histograms of cQDs in DMEM at 24 h, 48 h, 72 h and 96 h. FL decay curves were fitted using a sum of 3 exponential functions, residuals and χ^2 values are presented.

Supplement 2: Investigation of CdSe QD-Ce6 complex

Example results from an earlier study involving formation of CdSe QD-Ce6 complexes are presented in Figs. S2.1. and S2.2.

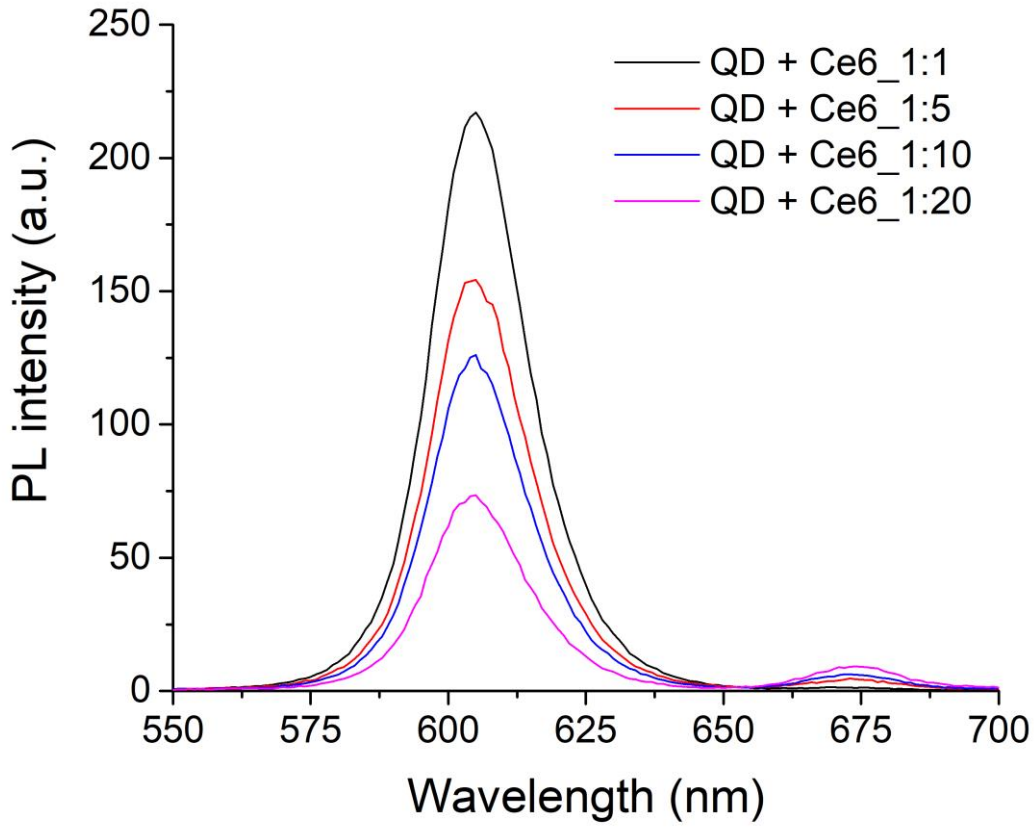

Figure S2.1. Fluorescence spectra of CdSe QD-Ce6 complexes formed with different QD:Ce6 ratios. Excitation light (470 nm) was absorbed by QDs, but not by Ce6. Complex formation is evidenced by Ce6 fluorescence band at 673 nm.

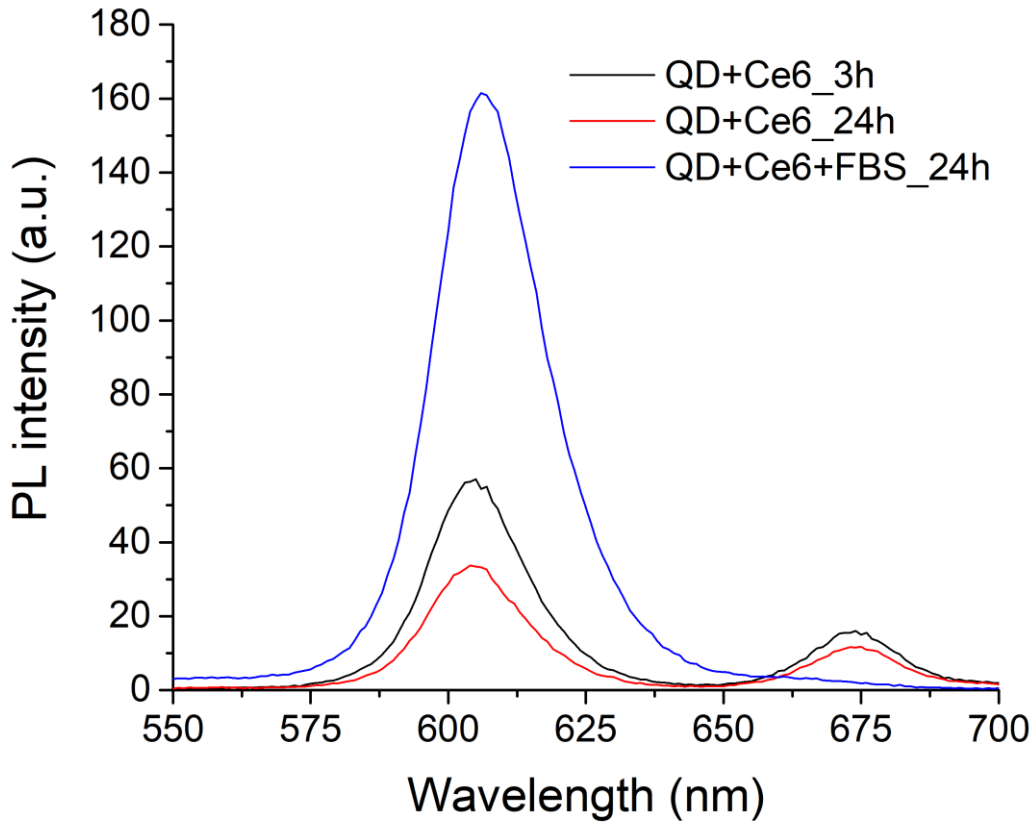

Figure S2.2. Fluorescence spectra of CdSe QD-Ce6 complex after formation (3 h) and after 24 h. Excitation light (470 nm) was absorbed by QDs, but not by Ce6. Disappearance of Ce6 fluorescence band at 673 nm after FBS was added shows that interaction with proteins disrupts the formed complex.

LIST OF PUBLICATIONS AND CONFERENCE PRESENTATIONS ON THE TOPIC OF THE THESIS

Publications:

1. Marin, R., Skripka, A., Huang, Y., Loh, T. A. J., Mazeika, V., Karabanovas, V., Chua, D. H. C., Dong, C., Canton, P. & Vetrone, F. Influence of halide ions on the structure and properties of copper indium sulphide quantum dots. Chem. Commun, 56, 3341-3344 (2020). https://doi.org/10.1039/C9CC08291C

Conference presentations:

1. Biocompatible and heavy metal free $CuInS_2$/ZnS quantum dots for cancer diagnostics. Poster presentation, Open Readings 2019. March 19-22, 2019, Vilnius, Lithuania.

2. Biologiškai suderinami $CuInS_2$/ZnS kvantiniai taškai vėžio diagnostikai. Poster presentation, Lithuanian National Physics Conference. October 3-5, 2019, Kaunas, Lithuania.

ACKNOWLEDGEMENTS

I wish to thank my supervisor Dr. Vitalijus Karabanovas and consultant Dominyka Dapkutė, as well as other members of Biomedical physics laboratory, for their help and support during this project. I also want to express my gratitude to Artiom Skripka and Vetrone group from the Institut National de la Recherche Scientifique of University of Quebec for the provided quantum dots.